Geochemical signatures of rare earth elements and yttrium in the vicinity of an ion-adsorption type deposit: roles of source sediment control

Haiyan Liu[1, 2, *]; Huaming Guo[3, *]; Olivier Pourret[4, *]; Maohan Liu[1, 2]; Zhen Wang[1, 2]; Weimin Zhang[1, 2]; Zebing Li[1, 2]; Bai Gao[1, 2]; Zhanxue Sun[1, 2]; Pierre Laine[4]

[1] *School of Water Resources and Environmental Engineering, East China University of Technology, Nanchang 330013, P. R. China*

[2]*State Key Laboratory of Nuclear Resources and Environment, East China University of Technology, Nanchang 330013, P. R. China*

[3] *School of Water Resources and Environment, China University of Geosciences (Beijing), Beijing 100083, P.R. China*

[4]*UniLaSalle, AGHYLE, Beauvais, France*

*** Corresponding authors:** Haiyan Liu hy_liu@ecut.edu.cn, Huaming Guo hmguo@cugb.edu.cn, Olivier Pourret olivier.pourret@unilasalle.fr

Abstract: The elevated concentrations of rare earth elements (REE) and yttrium (REE+Y) in acid mine drainage (AMD) constitute an opportunity for REE+Y recovery. However, the source and control of REE+Y signatures in AMD remains uncertain. Water, rock, sediment and sludge samples were collected from an ion-adsorption rare earth mining area to investigate REE+Y concentration and fractionation patterns in AMD. High concentrations of REE+Y occur in the pristine mine water (MW), and decrease progressively with MW passing through nitrification-denitrification (NDT) and coagulating-precipitation (CPT) treatment procedures in a water treatment plant. Concentrations of REE+Y are 1 to 3 orders of magnitude higher in MW, NDT and CPT samples than those in well water (WW), and are negatively correlated (R^2 0.72) with pH (3.8 to 8.7), suggesting that an enhanced acidic dissolution of minerals contributes REE+Y to AMD from the source area. Speciation calculation indicates that REE+Y are mainly free ions and sulfate complexes in MW and NDT samples, while carbonato and dicarbonato complexes in CPT samples. Normalized REE+Y patterns of water samples show a coherent enrichment of heavy REE (HREE) over light REE (LREE) and negative Ce anomalies. HREE-enriched patterns and Ce anomalies are kept relatively constant in MW, NDT and CPT samples, despite their huge disparity in REE+Y concentrations, indicating a limited impact of preferential precipitation of LREE over HREE on REE+Y fractionations. The HREE-enriched patterns possessed by AMD are similar to those of sediment samples, while are distinct from whole rocks. These behaviors suggest a major role of sediment source in controlling REE+Y concentrations and patterns in AMD. Results of XRD show abundance of muscovite, kaolinite and feldspar in sediments. Combining to SEM-EDS examinations, minerals such as kaolinite, schwertmannite ($Fe_{16}O_{16}(SO_4)_3(OH)_6(H_2O)_{10}\cdot 10H_2O$) and ferrihydrite are suggested to be the main hosts of REE+Y in sediments. Hence, HREE-enriched patterns of AMD result from preferential leaching of HREE from sediments which accumulate REE+Y after being initially mobilized from rocks under the conditions prevailing in mine site. The free form and sulfate complexation preserves REE+Y patterns and facilitates REE+Y mobility in the AMD system. Based on the plant treatment capacity, the potentially recoverable LREE and HREE are

calculated to range between 1116 g/day and 3373 g/day, and between 1288 g/day and 3764 g/day, respectively.

Keywords: Lanthanide; Acid mine drainage; Water-rock interaction; Fractionation; Critical metals

1. Introduction

Acid mine drainage (AMD), which is generated through oxidation of sulfides (i.e. pyrite) containing in target strata upon exploitation and exposure to oxygenated environment in mine sites, has acidic pH and contains elevated sulfate and metal(loid)s (Nordstrom and Alpers, 1999; Gimeno et al., 2000; Nordstrom, 2011). The highly polluted AMD has been considered a severe environmental problem posing great risks to surroundings and residents living near the exploited mine. This issue has been flagged as a global concern (Akcil and Koldas, 2006), particularly in those countries and regions with long-term large-scale open-pit mining activities (e.g. China, Vietnam, Australia, India and Spain) (Marquez et al., 2018 and references therein). The AMD could be treated by passive technology driven by natural forces like dissolution and microbial activity or by active technology which requires external input of energy and material to maintain the continuous operation (Johnson and Hallberg, 2005). However, both technologies have drawbacks, such as clogging problem resulting from mineral precipitation for the former and costly and time-consuming for the latter (Léon et al., 2021).

Acid mine drainage has also been shown to contain high levels of rare earth elements (REE) and yttrium (REE+Y) (Verplanck et al., 2004). The coherently chemical properties and predictable behaviors of REE+Y make them ideal recorders of clastic sediment transport (Taylor and McLennan, 1988), water-rock interactions of aquatic system (Worrall and Pearson, 2001), and mixing processes (Liu et al., 2017). Owing to their spectroscopic and magnetic properties, the REE+Y have been widely used in metallurgy, optics, catalyzing chemistry, electronics, clear energy producing, medical diagnosis and other various applications (Wall, 2014; Van Gosen et al., 2014). This has entailed an increasing demand for REE+Y and a growing supply for the world’s market. Therefore, seeking alternative sources of REE+Y especially HREE (i.e. Dy, Tb, Eu and Yb) is in urgent need for development of technology in many countries (Binnemans et al., 2013). Indeed, REE+Y recovery from AMD and its sludge have been investigated by a vast number of studies (Ayora et al., 2016; Stewart et al., 2017; Vass et al., 2019; Zhang and Honaker, 2020).

Previous researches on the concentration and distribution of REE+Y in AMD of various mine sites show that the REE+Y concentrations in AMD are several orders of magnitude higher than the median values of near-neutral waters (Ayora et al., 2016), and the normalized REE+Y patterns (with respect to standards such as North American Shale) are characterized by middle REE (MREE: Sm to Dy) enrichment over light REE (LREE: La to Nd) and heavy REE (HREE: Ho to Lu). The MREE-enriched REE+Y patterns were shown to exhibit differently from patterns of rock/sediment that AMD flow through and have been documented in many studies (Olías et al., 2005; Silva et al., 2009; Delgado et al., 2012; Sahoo et al., 2012; Stewart et al., 2017). However, LREE- (Bozau et al., 2004) and HREE- (Medas et al., 2013) enriched patterns were also observed in AMD, and enrichments of both MREE and HREE in acidic systems have been reported as well (Gammons et al., 2003; Sharifi et al., 2013; Migaszewski et al., 2014).

In spite of the known normalized REE+Y patterns in AMD systems, the underlying mechanism regulating the formation of the patterns is poorly understood. Considering the extremely low concentrations of REE+Y in rainwater (Zhang and Liu, 2004; Zhu et al., 2016), REE+Y are ultimately sourced from rocks which fluids move through. Studies have proposed a preferential leaching of REE-bearing solid phases to be a cause for the enrichment patterns (Sun et al., 2012a; Wallrich et al., 2020 and references therein). In this framework, corresponding REE+Y-enriched mineral phases should present in the bulk solid samples. Sequential extraction techniques using carbonate and silicate with solution pH of 1.6, 3.6 and 5.5 were performed to stimulate formation process of acidic groundwater, showing that the sequential extracts have similar REE patterns to those of AMD (Worrall and Pearson, 2001). Results of the author's experiments suggested that REE signatures in acidic water were a mixture of leachates of various sedimentary components. This means that REE+Y enrichment patterns are of source-control and local strata lithologies play a significant role in contribution of REE+Y to AMD. Furthermore, the conservative behaviors of REE+Y in the acidic solutions have accounted for their long-distance transport (Verplancket al. 2004). However, other studies indicate that process-derived

reactions such as fractionation of colloidal complexes (Åström and Corin, 2003), adsorption-desorption on surface coatings (Åström, 2001), differences in solution complexation (Dia et al., 2000; Zhao et al., 2007), and preferential precipitation of certain REE during formation of secondary minerals (Elderfield et al., 1990; Leybourne et al., 2000) are responsible for the REE+Y enrichment patterns. A recent study suggested that the roles of geology in controlling REE+Y distribution and patterns in AMD might be complicated by geochemical, biological and environmental factors (León et al., 2021). The unique properties of REE+Y constitute an opportunity to study the source, origin, fate and transport of AMD, which is important in addressing the mechanisms of AMD formation and contamination.

Therefore, the objectives of this study are to: (i) investigate the concentrations and distributions of REE+Y in AMD, (ii) characterize the geochemical controls on REE+Y sources and fractionation patterns in AMD, and (iii) assess the feasibility of REE+Y recovery from AMD.

2. Method and materials

2.1 Regional hydrogeological settings

The mining site (longitude: 114°47′28″, latitude: 24°54′25″) is located in the Jiangxi province, southern China. It has a subtropical monsoon climate characterized with plentiful rainfall and abundant sunlight. The highest temperature recorded historically is 39 °C and the lowest is -3.1 °C. The annual average temperature is 19.7 °C. Precipitation ranges from 1058 to 2190 mm (annual average 1608 mm), dominating from April to July (accounts for 60%). Annual evaporation is 1497 mm (ranging between 1349 mm and 1619 mm), intensely occurring in July and August. The drainage systems are well developed in the basin and have five main rivers, which are connected to the tributaries of Dongjiang River running from south to north with a flow rate of 13.93 m^3/s.

Strata of Senonian to Quaternary well outcrop in the mine area. The Cambrian, Devonian and Jurassic strata have the largest exposed area and are mostly distributed in eastern and southern part. The mine area is hosted in Jurassic to early-Cretaceous igneous rocks, which are mainly composed of acidic granites and cover a total area of 359 km^2. The main rocks are micaceous granite, granite porphyry, monzonitic granite and diorite (Yang et al., 2013). The REE+Y are originally born in two types of rocks, namely muscovite granite and biotite granite, where HREE and LREE have distinct fractions in the completely weathering layers (Yang et al., 2013). The HREE were shown to account for 75% to 89% (wt) with an average ratio of HREE to LREE (HREE/LREE) being 4.4 in the residues of muscovite granite. The average HREE proportion was 61%, and the HREE/LREE value was 1.6 for biotite granite counterpart. Among the HREE, the Y occurs as Y_2O_3 and increases with increasing grade of rare-earth rocks with the largest fraction being commonly >50%. These rocks have experienced different extends of weathering. The thickness of strong-weathered layer ranges from 5 to 25 m. Minerals including quartz, feldspar and mica mainly occur in the weathering residues. Those rock bodies having undergone intense weathering exhibit sound permeability and become water conduits.

Weathering fissure water is the major groundwater source in the mine area. It is mainly hosted in the fissure network of medium-grain micaceous granite and largely belongs to phreatic water. The weathering crust has a depth of 7.6 to 25.4 m. The coefficient of permeability ranges between 0.13 and 0.19 m/d. Hydrochemical facies include Ca-SO_4, Ca-SO_4-HCO_3, Ca-Cl and Ca-HCO_3-Cl with total dissolved solids (TDS) from 17 to 170 mg/L. Aquifers are mainly recharged by precipitation and discharged via springs and/or seepage. Runoffs are controlled by distributions and occurrences of fissures. Hydrologic units form in the piedmont area leading to interactions between surface water and groundwater. There is no centralized groundwater source for drinking water supplies 100 km downstream of the mining area. Hence, groundwater is utilized in a decentralized way by inhabitants living nearby. Surface water is used for industry, irrigation and landscape entertainment.

Open pit was used to be an active mining operation in exploring rare-earth metals in this mine site; whereas now, underground shafts are mainly being used as well. During the former operation, the intense weathered crusts are excavated resulting in outcrops of the bedrock underlain, which thus modify the pristine hydrogeologic connections. The underground shaft technology is not easy to implement, because leaching solutions infiltrate into grounds and percolate with water flowing, generating environmental contaminations. Ammonium has been reported to exceed the threshold recorded in groundwater quality standard due to usage of ammonium sulfate as a leaching liquor (Liu et al., 2019). Additionally, slags and waste dumps produced over mining activities are potential risks to the surrounding rivers, especially during rainy seasons. In this respect, a sewage treatment plant (STP) was established in the piedmont area to receive fluxes of leaching solutions from the mine (Fig. 1). The treated water is discharged into rivers down-gradient.

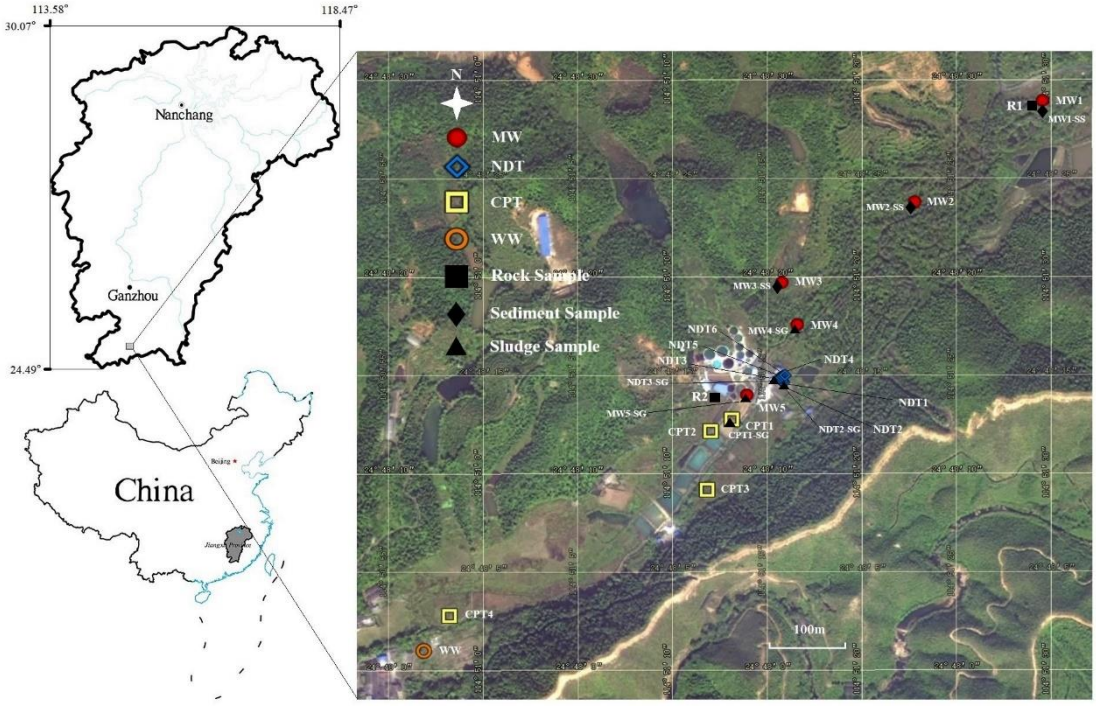

Figure 1 Study area and sampling locations (MW: pristine mine water sample; NDT: sample from nitrification-denitrification treatment process of a treatment plant; CPT: sample from coagulating-precipitation treatment process of a treatment plant: WW: well water sample; R: rock sample; SS: sediment sample; SG: sludge sample)

2.2 Sample collection

Sixteen water samples were collected in July 2020. Among them, four were pristine mine water samples (MW1 to MW5), six were effluents of STP undergoing nitrification-denitrification treatment procedures (NDT1 to NDT6), four were effluents going through coagulating-precipitation treatment processes (CPT1 to CPT4), and one was a well water (WW) collected from a local well in a village near the mine. The mine water is discharged after being treated via nitrification-denitrification and coagulating-precipitation processes. All water samples were filtered with 0.22 μm pore size cellulose acetate membrane filters. Samples for cation and trace element analysis were stored in 50 mL high-density polyethylene (HDPE) bottles and were acidified to pH< 2 with HNO_3. Samples for anion analysis were stored in the HDPE bottles without acidification. Samples for dissolved organic carbon (DOC) analysis

were sampled in 30 mL amber glass bottles and immediately acidified to pH < 2.0 by dropping 1:9 (volume) H_2SO_4. Samples for REE and Y analysis were sampled in 500 mL HDPE bottles following an acidification with HNO_3. All sampling locations are shown in the Fig.1.

Solid samples including two rock samples, three surface sediment samples and five sludge samples were collected. Rock samples (R1 and R2) were sampled from the mining area. Three surface sediment samples (MW1-SS, MW2-SS and MW3-SS) were collected corresponding to the locations where mine water samples (MW1, MW2 and MW3) were taken. Sludge samples (MW4-SG, MW5-SG and CPT1-SG) were sampled by taking the precipitates from bottom of the settling pond and creekbed, and NDT2-SG and NDT3-SG were sludge samples collected by using a long sucker. All the rock, sediment and sludge samples were stored in the clean plastic bags and placed in the shaded environment.

2.3 Analytical methods

Parameters, including temperature, pH, Electrical Conductivity (EC), and redox potential, were measured with a HI 9828 portable multi-meter (HANNA, Woonsocket, RI, USA) during water sampling. To minimize the influence of atmospheric contact, the monitoring probe was immersed in an in-line flow cell where water flows through constantly. Physiochemical data were recorded when stabilized. Alkalinity was titrated immediately in the field by using a Model 16900 digital titrator (HACH, Loveland, USA) during sampling. Redox sensitive components such as total Fe, Fe(II), NH_4-N, NO_2-N and S^{2-} were quantified using a portable UV/VIS spectrophotometer (HACH, DR2800).

Anions (SO_4^{2-}, NO_3^- and Cl^-) were analyzed by an ion chromatography system (ICS2000, Dionex, Thermo Fisher Scientific, Waltham, USA). Cations (K^+, Ca^{2+}, Na^+ and Mg^{2+}) and trace elements were determined by using ICP-AES (iCAP6300, Thermo Fisher Scientific, Waltham, USA) and ICP-MS (7500C, Agilent Technologies, Santa Clara, USA), respectively. The obtained results were verified to ensure the

analytical precision better than 5%.

Analysis of REE+Y concentrations were performed by employing two single-collector ICP-SFMS instruments (ELEMENT XR and ELEMENT 2, Thermo Fisher Scientific, Bremen, Germany) based on the protocol documented in Rodushkin et al. (2018). Cation exchange resin AG 50W-X8 (200 to 400 dry mesh size, Bio-Rad laboratory AB, Solna, Sweden) was used for preconcentration of REE+Y. Prior to use, the resins were immersed in 14 mol/L HNO_3 for a night and were cleaned with deionized water. A 2 mL low-density polyethylene (LDPE) column was loaded with the prepared resins, and 4 mL 14 mol/L HNO_3, 8 mL deionized water and 4 mL 9.5 mol/L HCl were loaded sequentially for conditioning. Finally, 200 mL sample was introduced into the pre-conditioned column and the retained REE+Y were eluted with 4 mL 0.5 mol/L HCl. By this method, a 50-fold preconcentration was achieved. The REE+Y recovery ranged between 90% and 103%. Calibration and quality control samples were prepared in 2% nitric acid with a stock solution. A medium resolution mode (MR, m/Δm approximately 5400) was set up for monitoring isotopes ^{146}Nd, ^{147}Sm, ^{151}Eu, ^{163}Dy, ^{165}Ho and ^{172}Yb, and a high resolution mode (HR, m/Δm approximately 12000) was used for monitoring isotopes ^{139}La, ^{140}Ce, ^{141}Pr, ^{157}Gd, ^{159}Tb, ^{166}Er, ^{169}Tm and ^{175}Lu, as suggested by Wilkin et al. (2020). The detection limits were 0.1 ng/L for Lu, 0.2 ng/L for Eu, and 0.5 ng/L for other REE and Y. In addition, 1 ng/L In solution was used as internal standard to check the stability of the analytical system. Interferences of BaO^+ on the ^{151}Eu and ^{153}Eu were corrected automatically by setting up a correction equation during analysis. Briefly, we run ~100 µg/L Ba and determine the peak area of the Eu isotope being monitored. During a run of samples, Ba (without calibration) was monitored and the results were applied for a correction. The analytical precisions of REE+Y were generally better than 8%.

Bulk composition analysis of sediment and sludge samples were carried out after a digestion using $LiBO_2$-LiB_4O_7 fusion/dilute nitric. The obtained solution was used for element determination by ICP-AES (iCAP6300, Thermo Fisher Scientific, Waltham, MA, USA) and ICP-MS (7500C, Agilent Technologies, Santa Clara, CA, USA). The oxides (SiO_2, Al_2O_3, Fe_2O_3, K_2O, MgO, MnO, Na_2O, P_2O_5 and TiO_2) were analyzed by

the X-ray fluorescence (XRF) (ARL Advant X) technique with a glass flux sheet method. Mineral compositions in surface sediments and sludges were determined by X-ray diffraction (XRD) (D8 advance, Bruker) equipped with a XGEN-4000 generator. Diffraction patterns for each sample were identified under operation condition at 40 kV and 40 mA, 2θ of 20° to 70°, and a step size of 0.02°. Minerals having content greater than 5 wt% of the bulk solid were identified.

The photomicrographic characteristics of the solid samples and residuals (by filtering water in-situ) of aqueous solution were examined by using scanning electron microscopy (SEM) and the elemental compositions were determined with energy-dispersive X-ray spectrometry (EDS, Jeol, Jsm-6510la).

2.4 Modelling approach

Speciation calculations were performed with hydrogeochemical code PHREEQC version 3.4 (Parkhurst and Appelo, 2013) using the Nagra/PSI database (Hummel et al., 2002). Stability constants of REE complexation to major anions (e.g. CO_3^{2-}, SO_4^{2-}, OH^-, Cl^-, F^-, and NO_3^-) were incorporated into the database. For examples, constants for $REE(CO_3)_2^-$ and $REECO_3^+$ were taken from Luo and Byrne (2004), and those for $REESO_4^+$ were from Schijf and Byrne (2004). Surface complexations of REE onto iron oxyhydroxides were considered as previously done by Liu et al. (2017), in which the relevant formation constants and detailed modelling procedures are provided.

3. Results

3.1 Water chemistry

The major ions and physicochemical parameters are shown in Table 1. Results show that pristine mine waters (MW1 to 5) have pH values between 3.8 and 4.2, showing a characteristic of acidic water. A slight increase in pH value (between 4.1 and 4.9) has been observed for NDT samples (NDT1 to 6). The CPT samples have pH values higher than 7 (between 7.4 and 8.7), and the WW sample's pH is 6.5. Generally, pH values increase from the regions nearest to the mine site to the downstream of the STP.

TDS range between 95 and 562 mg/L (average 363 mg/L) with the lowest values being found in WW. Before passing through the STP (i.e. MW1 to 5), sample cation is predominated by Ca^{2+} and Mg^{2+}, and HCO_3^- and SO_4^{2-} are the dominant anions. The Cl^- concentrations are below 6 meq%. Water types thus are Ca/Mg-HCO_3/SO_4 and Ca/Mg-SO_4. Over the CPT pathway (CPT1 to 4), the major cation shifts towards Na^+ (meq from 36% to 50%), followed by Mg^{2+} (meq ranging from 23% to 34%) and Ca^{2+} (meq from 22% to 25%), while the dominant anion is HCO_3^- (meq >62%), hydrochemical type for these samples being Na-Ca/Mg-HCO_3. This type of water stretches to the downstream near the village (CPT4), approximately 1 km downstream from the STP. The NDT samples have coherent water type of Mg-Na-Ca-HCO_3-SO_4. The WW collected from the village shows a Na-HCO_3 water type. All water compositions are shown with a piper plot for a comparison (Fig. 2).

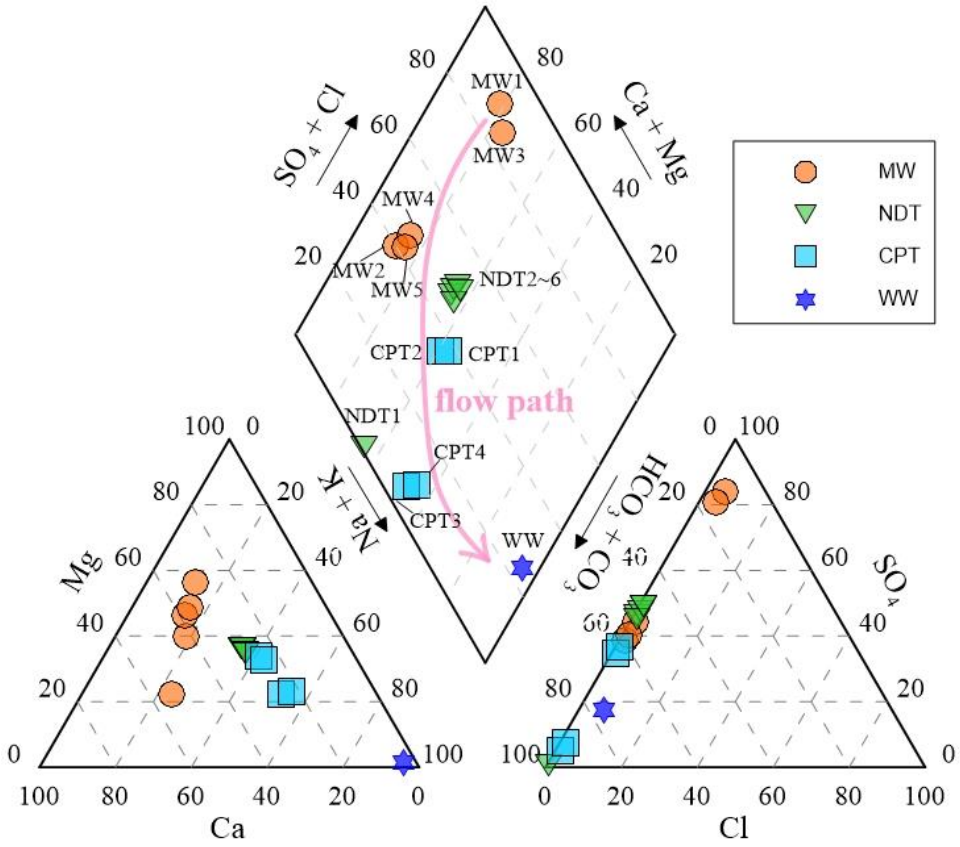

Figure 2 Piper plot of water samples

Total dissolved Fe (Fe_T) concentration ranges from 0.23 to 0.48 mg/L (average 0.31 mg/L) in MW samples, while it dramatically decreases to a range of 0.05 to 0.20 mg/L (average 0.08 mg/L) after passing through NDT procedure. A further decease in Fe_T concentration occurs in water going through CPT (0.03 to 0.07 mg/L, average 0.06 mg/L). Total dissolved Fe has the lowest concentration in WW (0.006 mg/L). Fe(II) generally dominates Fe species in MW and NDT water samples, as reflected by Fe(II) concentrations from 0.22 to 0.48 mg/L and from 0.01 to 0.08 mg/L, respectively. For CPT and WW samples, Fe(II) concentrations are below detection limits, with an exception of CPT4 which has Fe(II) concentration of 0.02 mg/L (Fig. 3a).

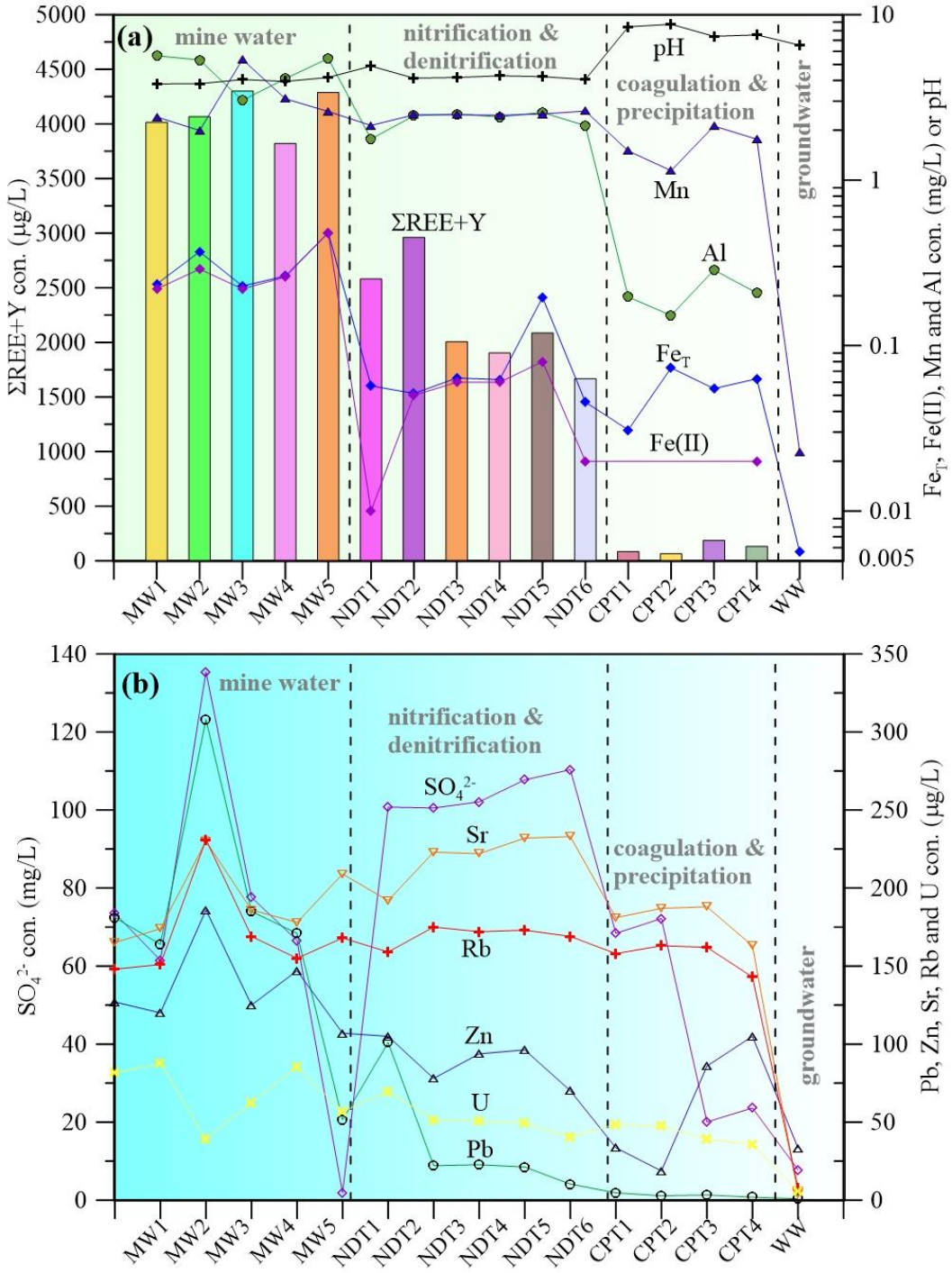

Figure 3 Changes of REE and Y with individual water samples ((a): pH, total REE and Y (∑REE+Y), total Fe (Fe_T), Fe(II), Al and Mn concentrations; (b): SO_4^{2-}, Sr, Rb, Zn, U and Pb concentrations)

The S^{2-} concentrations mostly are below detection limit. Among MW samples, only MW1 and MW4 have S^{2-} concentrations of 1 mg/L and 5.00 mg/L, respectively. All NDT samples are below detection limit for S^{2-} concentrations. The CPT samples

have S^{2-} concentrations below detection limit with an exception of CPT3 and CPT4 (3.00 mg/L). The WW sample has S^{2-} concentrations of 1 mg/L (Table 1).

Table 1 Physiochemical parameters (including pH, EC, TDS major ions and trace elements) of water samples (Pb, Zn, Sr, Rb and U: μg/L; other constituents: mg/L; "-"indicates beyond detection limits)

sample ID	MW1	MW2	MW3	MW4	MW5	NDT1	NDT2	NDT3	NDT4	NDT5	NDT6	CPT1	CPT2	CPT3	CPT4	WW
pH	3.8	3.8	4.1	4.0	4.2	4.9	4.1	4.2	4.3	4.2	4.1	8.5	8.7	7.4	7.6	6.5
Cl^-	3.4	1.7	5.5	1.8	2.1	0.8	1.8	1.9	1.8	2.7	1.9	1.8	1.7	3.9	3.6	2.2
SO_4^{2-}	73.5	61.5	135.4	77.6	66.6	1.9	100.7	100.5	102.1	107.7	110.3	68.4	72.2	20.0	23.6	7.8
NO_3^-	89.1	131.9	83.6	105.5	100.2	4.9	105.9	105.2	108.4	107.5	107.6	104.3	104.2	101.7	92.7	27.9
HCO_3^-	12.1	121.0	31.0	121.0	121.0	321.0	146.0	137.0	131.0	161.0	141.0	161.0	156.0	483.9	242.0	21.0
Ca	31.2	34.0	42.4	34.5	33.8	35.1	38.7	38.2	38.0	39.6	39.9	31.7	31.0	47.5	36.6	1.0
K	14.2	13.5	24.9	14.2	13.3	12.9	14.0	13.6	13.1	13.7	13.2	12.6	12.3	18.4	16.4	4.3
Mg	18.0	37.7	10.4	24.9	27.6	26.8	29.2	28.9	29.1	29.7	29.5	25.5	25.0	25.3	22.9	0.3
Na	7.73	8.59	6.59	7.38	8.91	42.53	45.91	45.26	46.67	51.72	52.16	51.82	55.69	103.56	95.05	30.31
TDS	243	349	324	326	313	285	409	402	405	433	425	377	380	562	473	95
TOC	1.6	2.6	1.5	1.5	3.2	2.1	1.8	1.4	1.9	2.2	2.4	2.3	2.4	10.8	8.3	1.1
Al	5.64	5.33	3.04	4.11	5.44	1.77	2.45	2.51	2.41	2.57	2.13	0.20	0.15	0.29	0.21	0.00
Fe(II)	0.22	0.29	0.22	0.26	0.48	0.01	0.05	0.06	0.06	0.08	0.02	-	-	-	0.02	-
Fe_T	0.24	0.37	0.23	0.26	0.48	0.06	0.05	0.06	0.06	0.20	0.05	0.03	0.07	0.05	0.06	0.01
Mn	1.96	1.83	4.58	2.61	2.11	2.11	2.01	2.13	2.12	2.17	2.32	1.28	1.05	1.89	1.58	0.01
S(II)	-	1.00	-	5.00	-	-	-	-	-	-	-	-	-	3.00	3.00	1.00
NH_3-N	11.8	12.1	12.5	11.6	13.2	10.2	11.1	12.0	12.0	12.1	9.9	11.1	-	8.9	9.0	0.2
NO_2-N	0.1	0.2	0.1	0.2	0.0	0.6	0.2	0.3	0.3	0.2	0.1	0.0	0.0	15.6	7.9	-
Zn	127	120	186	125	147	107	105	78	94	96	70	34	19	86	105	33
Sr	165	174	230	186	178	209	192	223	222	232	233	181	187	188	163	4
Rb	148	151	231	169	155	168	159	175	172	173	169	158	163	162	143	8
Pb	181	164	308	185	171	52	101	22	23	21	10	4.7	2.8	3.3	1.9	0.9
U	33	35	16	25	34	23	28	21	20	20	16	19	19	16	14	2.4

Total dissolved Al (Al_T) concentration ranges between 3.04 and 5.64 mg/L (average 4.7 mg/L) and between 1.77 and 2.57 mg/L in MW and NDT samples, respectively. It decreases to below 0.3 mg/L in CPT samples. The Al_T is not detected in WW. Total dissolved Mn (Mn_T) concentrations are generally higher in MW (between 2.00 and 5.36 mg/L, average 3.09 mg/L) samples, as compared to those in NDT (2.14 to 2.61 mg/L, average 2.45 mg/L) and CPT (1.14 to 2.12 mg/L, average 1.63 mg/L) samples. Other trace elements, including Pb, Zn, Sr, Rb and U, all decrease substantially after CPT procedures (Fig. 3b).

Total dissolved carbon (TOC) concentrations range from the lowest values in WW

(1.47 mg/L) to the highest values in CPT3 (10.96 mg/L) with an average value of 3.21 mg/L. Inorganic carbon dominates carbon species with concentrations from 1.08 to 10.75 mg/L (average 2.93 mg/L).

3.2 Aqueous REE+Y signatures

Total concentrations of REE+ Y (ΣREE+Y) in water samples are presented in Table 2. The ΣREE+Y concentrations range from 3837 to 4327 µg/L (average 4115 µg/L), and from 1674 to 2971 µg/L (average 2208 µg/L) in MW and DNT samples, respectively. These values are 1 to 2 orders of magnitude higher than the ΣREE+Y concentrations of CPT sample (65 to 188 µg/L, average 118 µg/L), and are more than 3 orders of magnitude higher than the ΣREE+Y concentrations of WW sample (5.34 µg/L) (Fig. 3a).

Upper Continental Crust (REE_{UCC}) normalized REE+Y patterns are characterized by HREE enrichment over LREE and negative Ce [$Ce/Ce^* = Ce_{UCC}/(La_{UCC} \times Pr_{UCC})^{0.5}$] and negative Eu [$Eu/Eu^* = Eu_{UCC}/(Sm_{UCC} \times Gd_{UCC})^{0.5}$] anomalies (Fig. 4). The $(Yb/Nd)_{UCC}$ is used as a fractionation measure to quantify REE+Y fractionation patterns. The $(Yb/Nd)_{UCC}$ values are higher in CPT samples (10.23, n=4) as compared to MW (7.11, n=5), NDT (7.76, n=6) and WW (5.70, n=1) samples. The Ce anomalies are below 0.3 with an exception of WW (Ce/Ce* 0.37). The average Eu/Eu* values are 0.47, 0.42 and 0.54 in MW, NDT and CPT samples, respectively. The WW sample has Eu/Eu* value of 0.71. The Y is plotted between Dy and Ho in the normalized REE+Y patterns due to their similar ionic radii (Fig. 4). Results show anomalous abundance of Y_{UCC} over its neighboring Ho_{UCC} in all samples. Ratios of Y_{UCC} to Ho_{UCC} of MW and NDT samples range between 1.14 and 1.53 (average 1.29), and between 1.21 and 1.36 (average 1.33), respectively. Values of $(Y/Ho)_{UCC}$ are greater than 1.70 for all CPT samples, and is 1.39 for WW sample.

Table 2 REE and Y concentrations (μg/L) and fractionation parameters (Eu/Eu*, Ce/Ce*, $(Er/Nd)_{UCC}$, $(Yb/Nd)_{UCC}$ and $(Y/Ho)_{UCC}$) of water samples

sample ID	MW1	MW2	MW3	MW4	MW5	NDT1	NDT2	NDT3	NDT4	NDT5	NDT6	CPT1	CPT2	CPT3	CPT4	WW
La	252	242	233	216	246	163	186	123	115	124	103	5.04	3.75	6.74	4.73	0.41
Ce	156	150	116	124	146	89	110	68	63	69	56	2.48	1.68	3.81	3.02	0.33
Pr	78	75	68	64	73	44	54	32	30	32	25	1.20	0.89	1.74	1.19	0.10
Nd	316	303	279	259	296	175	218	128	119	130	102	4.95	3.64	7.32	4.97	0.39
Sm	170	163	136	133	155	87	115	62	59	65	50	2.17	1.70	3.74	2.43	0.17
Eu	16	15	26	17	16	9.0	11	6.8	6.5	6.9	6.6	0.30	0.24	0.57	0.36	0.03
Gd	233	221	215	192	218	127	162	96	89	96	78	3.33	2.48	6.11	4.06	0.23
Tb	52	51	47	44	51	29	37	22	21	23	18	0.74	0.56	1.52	1.00	0.06
Dy	324	320	300	287	332	183	230	146	138	151	121	4.99	3.75	10.90	7.29	0.33
Ho	62	62	59	57	65	37	45	29	28	31	25	1.09	0.82	2.49	1.77	0.07
Er	183	187	169	166	193	110	132	88	85	95	74	3.32	2.48	8.13	5.67	0.20
Tm	27	28	23	24	29	16	20	13	12	14	11	0.47	0.35	1.23	0.87	0.03
Yb	186	191	139	161	198	102	132	83	82	92	71	3.02	2.24	7.93	5.74	0.19
Lu	27	28	20	23	29	15	19	12	12	13	10	0.43	0.33	1.15	0.84	0.03
Y	1932	2031	2472	2055	2241	1394	1490	1096	1044	1144	917	51	39.7	124	88.3	2.72
∑REE	2081	2034	1829	1765	2046	1186	1470	910	859	941	750	34	25	63	44	2.57
∑REE+Y	4013	4065	4301	3820	4287	2580	2960	2006	1903	2085	1667	85	65	187	132	5.29
Ce/Ce*	0.25	0.25	0.21	0.24	0.25	0.24	0.25	0.25	0.25	0.25	0.25	0.23	0.21	0.25	0.29	0.37
Eu/Eu*	0.38	0.37	0.70	0.49	0.40	0.40	0.39	0.41	0.42	0.41	0.50	0.52	0.55	0.56	0.53	0.71
$(Er/Nd)_{UCC}$	6.55	6.98	6.85	7.25	7.37	7.11	6.84	7.73	8.03	8.24	8.21	7.58	7.70	12.56	12.90	5.71
$(Yb/Nd)_{UCC}$	6.96	7.45	5.89	7.35	7.91	6.89	7.16	7.70	8.17	8.39	8.24	7.21	7.27	12.80	13.65	5.70
$(Y/Ho)_{UCC}$	1.14	1.20	1.53	1.32	1.26	1.36	1.21	1.36	1.36	1.35	1.36	1.70	1.76	1.81	1.81	1.39

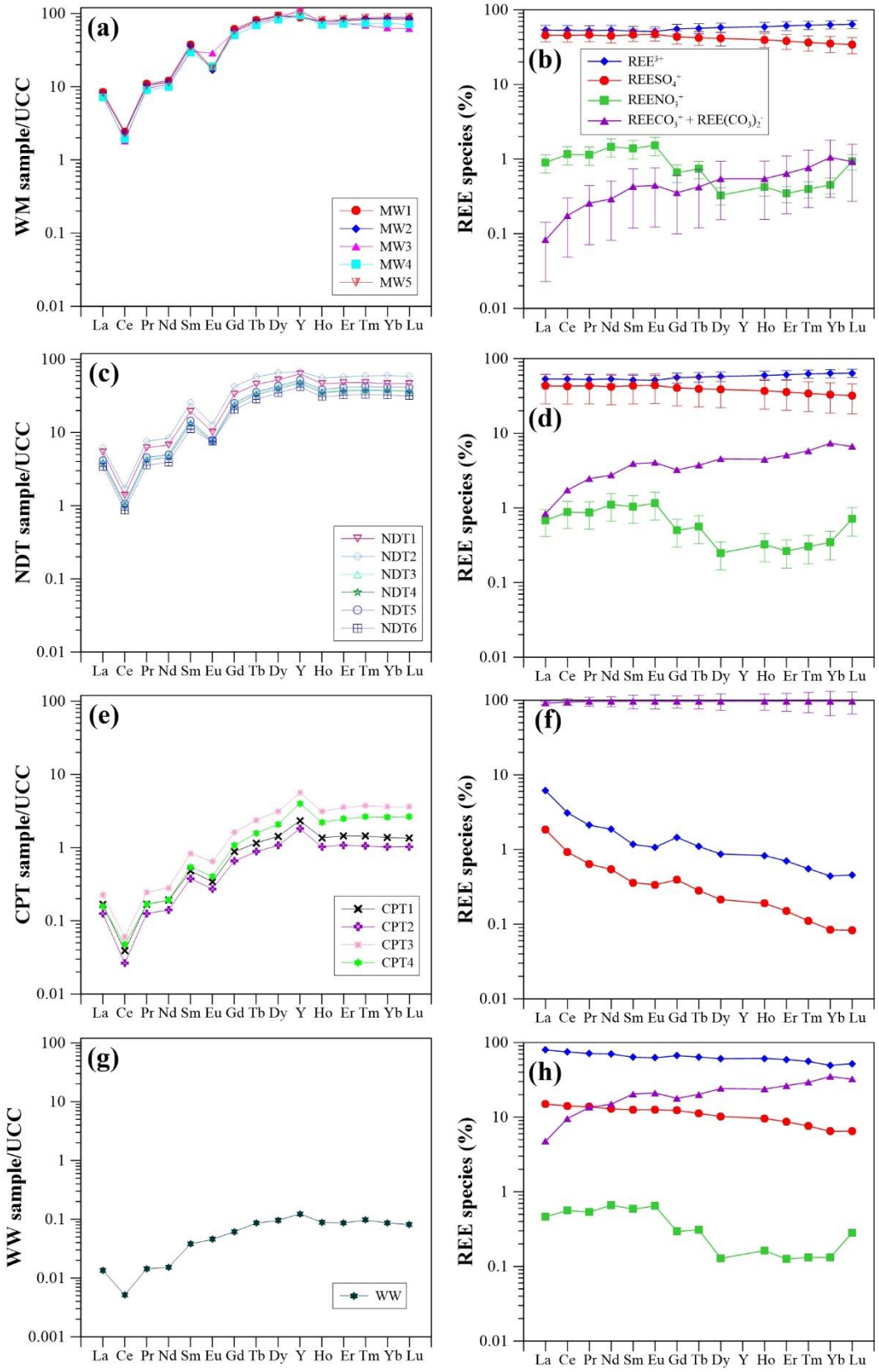

Figure 4 Upper Continental Crust (UCC) normalized REE+Y patterns for water samples and speciation modeling results ((a) and (b): MW sample; (c) and (d): NDT sample; (e) and (f): CPT sample; (g) and (h): WW sample)

3.3 Modelling results

The calculated lanthanide species are presented as a function of their atomic numbers (Fig. 4). Free (REE^{3+}) and sulfate ($REESO_4^+$) complexes dominate lanthanide species in MW and NDT samples. The LREE more tend to be associated with SO_4^{2-} and the HREE present as free ions. The average proportion of La occurring as $REESO_4^+$ is 48%, and 36% for Lu. Carbonate [$REECO_3^+$ and $REE(CO_3)_2^-$] and nitrate complexes ($REENO_3^+$) make up below 5% of the lanthanide species (Figs. 4b and d). The lanthanides in CPT samples are mainly in forms of $REECO_3^+$ and $REE(CO_3)_2^-$, which account for 73% to 98% for La and 89% to 99% for Lu. Free ion makes up 6% for La and blow 1% for Lu (Fig. 4f). Lanthanides are predicted to occur as free ions, $REECO_3^+$ $REE(CO_3)_2^-$, and $REESO_4^+$ in WW sample. The proportions of these three species are predicted to be 49% to 79%, 5% to 34%, and 7% to 15%, respectively (Fig. 4h). $REENO_3^+$ mostly accounts for below 2% of total lanthanide species. The other species, including hydroxyl and chloride complexes, are below 1% in all water samples.

3.4 Geochemical and mineralogical properties of solids

The chemical compositions of rock, surface sediment and sludge samples are presented in Table 3. Results show that rock samples are dominated by SiO_2 (66 wt% to 68 wt%). Aluminum oxide (Al_2O_3) is the second abundant component (9 wt% to 18 wt%), followed by Fe_2O_3 (3.66 wt% to 7.39 wt%), K_2O (1.89 wt% to 4.08 wt%) and CaO (1.33 wt% to 5.08 wt%). Other metal oxides, including MgO, Na_2O, TiO_2 and MnO, have contents below 2 wt%. The loss on ignition (LOI) ranges between 3.25 wt% and 3.33 wt%. Composition of surface sediment samples ranges from 61 wt% to 76 wt% for SiO_2, 9.96 wt% to 2.63 wt% for Al_2O_3, 2.11 to 4.78 wt% for Fe_2O_3, 2.11 to 4.79 wt% for K_2O, and 6.7 to 8.09 wt% for LOI. Contents of CaO, MgO, Na_2O, TiO_2, MnO and P_2O_5 are below 1 wt%. Sludge samples have contents of SiO_2 ranging from 60 to 67 wt%, Al_2O_3 from 14.87 to 17.95 wt%, Fe_2O_3 from 3.17 to 12.18 wt%, K_2O from

1.14 to 4.49 wt%. Metal oxides, including CaO, MgO, Na_2O, TiO_2, P_2O_5 and MnO, are below 3 wt%. Geochemical characteristics of solid samples vary from superficial to subsurface samples.

Table 3 Chemical compositions of solid samples (oxides and LOI: wt%; trace elements: mg/kg)

	sediment sample			sludge sample					rock sample	
component	MW1-SS	MW2-SS	MW3-SS	MW4-SG	MW5-SG	NDT2-SG	NDT3-SG	CPT1-SG	R1	R2
SiO_2	75.59	60.59	68.53	63.47	66.62	60.22	63.87	59.62	67.74	66.35
Al_2O_3	9.96	22.63	14.81	17.70	17.19	14.87	17.21	17.95	9.39	17.97
CaO	0.07	0.07	0.08	0.10	0.78	2.56	1.20	1.00	5.08	1.33
Fe_2O_3	2.10	3.97	4.78	3.17	5.33	9.72	8.64	12.18	7.39	3.66
K2O	4.79	4.01	2.11	4.49	1.14	1.69	1.18	1.65	1.98	4.08
MgO	0.10	0.32	0.33	0.27	0.63	2.14	0.98	1.07	0.48	1.46
MnO	0.03	0.03	0.03	0.03	0.15	0.20	0.18	0.53	0.16	0.05
Na_2O	0.25	0.15	0.05	0.36	0.15	0.75	0.28	0.10	1.69	0.09
P_2O_5	0.02	0.04	0.06	0.06	2.58	1.69	1.81	2.62	0.20	0.15
TiO_2	0.15	0.31	0.65	0.32	0.44	1.32	0.65	0.41	0.58	1.03
LOI	6.74	8.02	8.10	10.56	5.51	4.17	3.08	3.33	3.25	3.33
Ag	0.07	0.09	0.06	0.1	0.51	0.29	0.3	0.2	0.11	0.05
As	5.4	13.7	11.3	8.1	70	22.8	70	8.9	4.7	9.4
Ba	161.5	173.5	235	154	261	395	322	17.0	334	783
Be	3.04	5.31	3.4	6.8	173	14.1	150.5	32.8	30.2	3.62
Cr	10	20	30	16	43	90	60	2.8	18	120
Cs	12.45	19.35	12.05	19.35	7.75	9.2	8.06	8.6	46.6	12.65
Hf	4.6	7.9	10.1	20.3	2.5	5.8	2.9	7.8	6.7	11.6
Li	54.6	84.7	42.8	77.4	36.7	45.3	42	53.0	104.5	35.3
Mo	0.69	1.46	0.78	0.9	2.89	5.67	2.83	2.3	1.48	0.45
Pb	58.8	114	107.5	111	1315	588	1280	256	19.8	16.3
Rb	525	465	224	593	110	102.5	98.9	325.0	247	249
Sc	5.8	14.7	12.8	9.8	10.1	15.2	11.5	10.0	9.3	16.5
Sn	23	31	15	43	12	12	15	5.0	5	8
Sr	15.4	18.4	16.5	16.6	72.1	285	123.5	5.1	90.3	58
Th	15.3	53.3	29.6	41.4	19.05	18.75	18.75	19.4	17.15	31.9
U	6.6	19.3	8.4	21.3	180.5	131.5	251	63.0	4.5	5.46
V	12	32	67	29	55	132	81	55.0	53	174
W	2.6	6	3.6	5.1	1.6	5.6	2.7	5.4	1.7	3.9
Zn	41	105	69	78	594	205	508	116.0	79	66
Zr	127	197	355	566	122	251	143	320.0	264	436

Contents of ΣREE+Y in sludge samples range between 797 and 44746 mg/kg with an average of 19952 mg/kg. Those values are higher than the ΣREE+Y contents of rock (325 to 845 mg/kg, average 655 mg/kg) and sediment samples (347 to 430 mg/kg, average 389 mg/kg) (Table 3). UCC-normalized REE+Y patterns show that all samples are enriched in HREE relative to LREE and have negative Ce and Eu anomalies. The $(Yb/Nd)_{UCC}$ values range from 6.14 to 9.14, from 3.51 to 5.83 and

from1.08 to 2.10 in sludge, sediment and rock samples, respectively (Table 4). The normalized REE+Y patterns of sludge and sediment samples exhibit an increasing upward trend from La to Sm, and a relatively flat trend from Tb to Lu (Fig. 5), while REE+Y patterns for rock samples show a slightly increasing trend with atomic numbers, indicating that a higher degree of HREE enrichment over LREE occurs for sludge and sediment samples as compared to rock samples. Cerium anomalies range from 0.18 to 0.63 and from 0.61 to 0.79 in sludge and sediment samples, respectively. Rock samples show weakly negative Ce anomalies (Ce/Ce* ~0.98). Europium anomalies range between 0.07 and 0.13, and between 0.09 and 0.22, and between 0.63 and 0.86 in sludge, sediment and rock samples, respectively. The $(Y/Ho)_{UCC}$ values are mostly greater than 1 (average 1.10), indicating a weakly positive Y/Ho anomalies in the solid samples (Table 3).

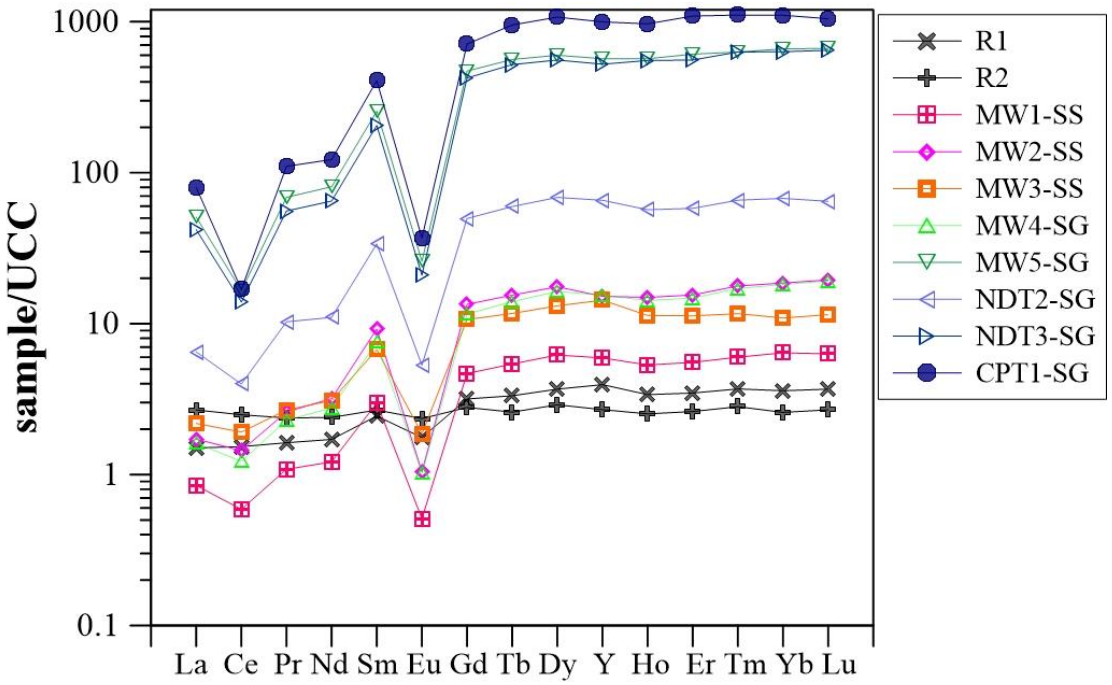

Figure 5 Upper Continental Crust (UCC) normalized REE+Y patterns for rock, sediment and sludge samples (R: rock; SS: sediment: SG: sludge)

Table 4 REE and Y contents (mg/kg) and fractionation measures in solid samples

	sediment sample			sludge sample					rock sample	
component	MW1-SS	MW2-SS	MW3-SS	MW4-SG	MW5-SG	NDT2-SG	NDT3-SG	CPT1-SG	R-1	R-2
La	25.4	51.6	65.5	48.7	1525	195	1260	2398	45.10	80.40
Ce	37.7	92.4	122.5	78.1	1060	255	891	1080	98.20	159.50
Pr	7.7	18.5	19.0	16.3	488	73	396	783	11.55	16.85
Nd	31.6	82.9	80.7	71.8	2100	286	1690	3179	44.50	62.20
Sm	13.4	41.5	30.3	34.0	1150	152	927	1835	11.00	12.05
Eu	0.5	0.9	1.6	0.9	22.8	4.7	18.4	32.5	1.55	2.07
Gd	17.8	51.0	40.5	44.0	1790	189	1612	2703	12.05	10.60
Tb	3.5	9.9	7.5	9.0	360	38	333	609	2.13	1.66
Dy	21.7	61.4	46.0	57.2	2100	240	1954	3757	12.90	10.15
Ho	4.3	12.0	9.1	11.4	455	46	443	775	2.71	2.02
Er	12.8	35.6	25.9	34.0	1404	134	1284	2508	7.98	6.02
Tm	2.0	5.9	3.8	5.6	208	22	208	366	1.22	0.93
Yb	14.1	40.9	24.0	40.0	1454	149	1393	2431	7.91	5.68
Lu	2.0	6.2	3.7	6.1	213	21	207	335	1.18	0.86
Y	131	334	315	340	12504	1445	11521	21956	87	59
∑REE	194	511	480	457	14330	1803	12616	22790	260	371
∑REE+Y	325	845	795	797	26834	3248	24137	44746	347	430
Ce/Ce*	0.61	0.68	0.79	0.63	0.28	0.49	0.29	0.18	0.98	0.99
Eu/Eu*	0.14	0.09	0.22	0.11	0.07	0.13	0.07	0.07	0.63	0.86
$(Er/Nd)_{UCC}$	4.56	4.85	3.63	5.35	7.56	5.28	8.59	8.92	2.03	1.09
$(Yb/Nd)_{UCC}$	5.27	5.83	3.51	6.58	8.18	6.14	9.74	9.04	2.10	1.08
$(Y/Ho)_{UCC}$	1.11	1.02	1.26	1.08	1.00	1.15	0.95	1.03	1.16	1.07

SEM examinations of filter residuals show that the mine waters contain many aggregates with diameters larger than 0.22 μm. This is more commonly observed in CPT samples as compared to MW samples (Fig. S1). Results of EDS show that peaks of Fe and Mn co-occur with these of O, and peaks of REE co-occur with those of Al (Fig. 6). Elemental composition determinations show that C and O account for 91% to 98%, reflecting the background matrix of the filter. Compositions of Fe, Mn and Al are below 1%. Contents of REE+Y range between 0.04% and 2.21% (average 0.63%) and between 0.02% and 2.27% (average 1.03%) in MW and CPT samples, respectively (Fig. 6).

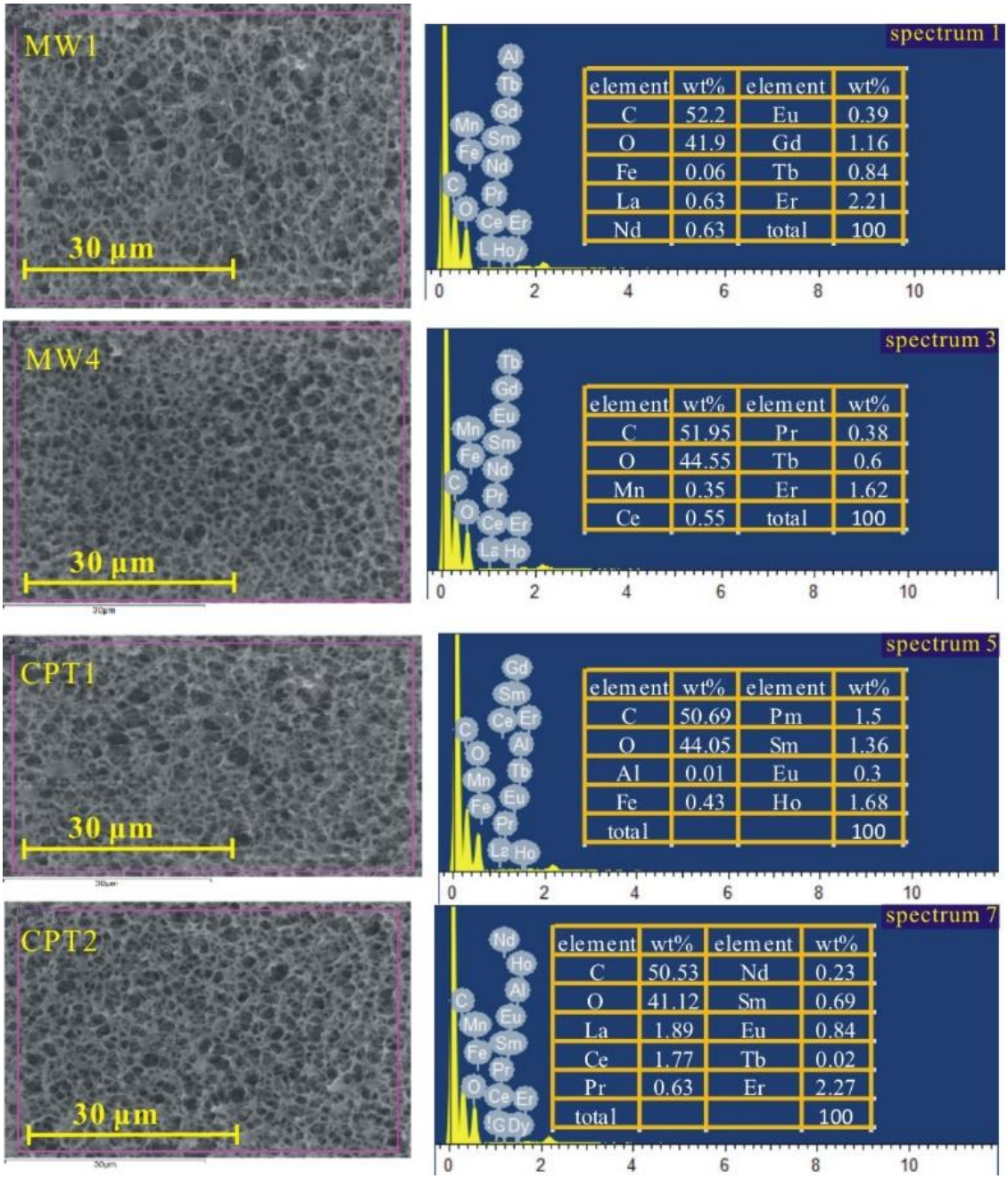

Figure 6 Results of SEM and EDS examination for residuals of MW and CPT samples

Results of XRD show that quartz (SiO_2), muscovite ($KAl_{2.2}(Si_3Al)_{0.975}O_{10}((OH)_{1.72}O_{0.28})$), kaolinite ($Al_4(OH)_8(Si_4O_{10})$), feldspar (albite ($Na(AlSi_3O_8)$) or microcline ($KAlSi_3O_8$)), schwertmannite ($Fe_{16}O_{16}(SO_4)_3(OH)_{10}\cdot 10H_2O$), and ferrihydrite ($Fe_{9.56}O_{14}(OH)_2$) are present in solid samples (Fig. S2). The percentages of these minerals are 56% to 68%, 7% to 11%, 8% to 14%, 10% to

14%, 3% to 4% and 3% to 5% in sediment samples, respectively. For sludge samples, these minerals account for 27% to 47%, below detect limitation to 11%, 10% to 27%, 15% to 24%, 4% to 9% and 1% to 5%, respectively.

SEM images of sediment and sludge samples are shown in Fig. 7 and Fig. S3. The sediment samples contain clastic textures on the surfaces with length < 1 μm. EDS spectra indicate that the stripe-like shapes are probably Al- and/or Fe-bearing crystals. The percentage of Al and Fe is determined to be 7% to 10% and ~2%, respectively. REE+Y are all below 1% with exceptions of Dy and Er (Fig. 7). On the surfaces of sludge samples, needlelike and burr-like shapes occur with shorter length than those observed in sediment samples. EDS results show that Al and Fe account for from 7% to 10% (average 10%) and from 1% to 8% (average 5%), respectively, indicating that these are the amorphous Al- and Fe-containing minerals.

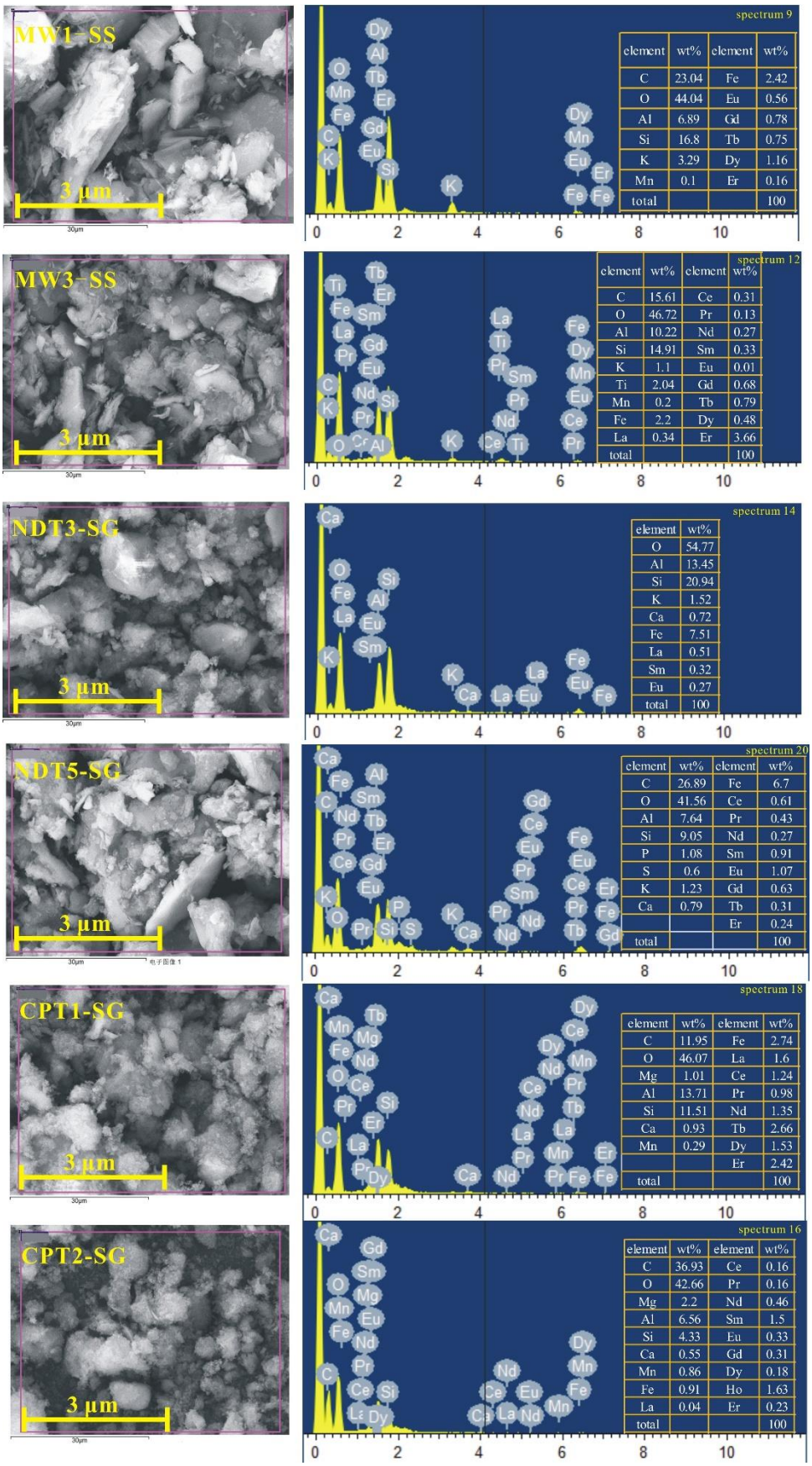

Figure 7 Results of SEM and EDS examination for sediment and sludge samples

4. Discussion

4.1 REE+Y occurrences and comparison with other mine sites worldwide

The acid waters have been shown to contain REE concentrations several orders of magnitude higher than the medians of natural near-neutral waters (Ayora et al., 2016). Comparing the results of this study with REE concentrations documented from other mine sites around the World shows that the total REE (ΣREE) concentrations of MW samples are relatively high, exhibiting the same order of the values reported by Migaszewski et al. (2016), Gammons et al. (2003) and Sharifi et al. (2013) (Table 5). The lowest ΣREE concentration (1782 μg/L) in MW sample is higher than the maximum values of most mine sites. These include the effluents discharged by an abandoned Zn-Pb mine (Santa Lucia) in western Cuba (370-860 μg/L) (Romero et al. 2010), AMD in the Iberian Pyrite Belt mine area, Portugal (Pérez-López et al., 2010), and surface waters of a Cu-Mo mine tailing pond, Mongolia (Munemoto et al., 2020). It is noteworthy that the ΣREE concentrations show a wide range from 0.17 to 13046 μg/L (average 1596 μg/L) with pH of 4.6 to7.4 in stream waters from a rare earth mine area, Southern China, which is the same ion-adsorption type deposit (Hao et al., 2016).

Co-occurrence of REE+Y with high levels of metal elements (i.e., Fe, Al and Mn) and SO_4^{2-} is an important feature for the investigated waters. The MW samples have much higher ΣREE+Y concentrations than treated waters and WW. With MW water moving downward, ΣREE+Y concentrations decrease (Fig. 3a). Trends of Fe, Al and Mn concentrations are similar to those of ΣREE+Y concentrations, indicating that REE+Y exhibit similar behaviors to Fe, Al and Mn. Indeed, the Fe, Al and Mn concentrations are positively correlated with ΣREE+Y concentrations with correlation coefficients (R^2) of 0.61, 0.86 and 0.43, respectively. Samples with relatively higher ΣREE+Y concentrations contains relatively higher SO_4^{2-} concentrations. Although only a weak positive correlation is observed between SO_4^{2-} and ΣREE+Y concentrations (R^2=0.18), the predominance of SO_4^{2-} in total anions can be observed in MW samples, and it shifts to the planted treated water samples (NDT and CPT) with water migrating downwards (Fig. 2). The predominance of SO_4^{2-} is related to the usage of ammonium

sulfate as an agent for REE+Y leaching during the mining. An examination of the literature dataset in acid waters indicates that ΣREE concentrations have positive correlations to Fe, Al, Mn and SO_4^{2-} concentrations (Fig. 8a, b and c). Positive correlations between Fe and Al and ΣREE+Y concentrations were found in AMD in a historical mining area (Moreno-González et al., 2020), although the high levels of SO_4^{2-} (average 27052 mg/L) and Mn (average 122.7 mg/L) were not highlighted by the authors. The mechanism for co-occurrence of REE+Y and Fe, Al and Mn are due to intense leaching of these cation ions. Some studies reported that REE+Y were scavenged by Fe, Al and Mn oxyhydroxides, which may also be one of reasons for their co-occurrences. Presence of SO_4^{2-} could be of both anthropogenic and natural processes (Liu et al., 2019). Further, SO_4^{2-} shows high affinities to REE+Y under acid conditions via complexation leading to enhanced migrations of REE+Y (Li and Wu, 2017). It should be noted that, in additional to Fe, Al and Mn, high concentrations of Zn (average 86.85 mg/L) and Ni (average 5.13 mg/L) are found to co-occur with REE+Y in AMD as well. These phenomena were observed in mine waters from Iberian Pyrite Belt (IPB) and Sarcheshmeh porphyry copper deposit (Léon et al., 2021; Sharifi et al., 2013). The present study reveals that the highest concentrations of Zn and Ni are 186 μg/L and 8.39 μg/L, respectively. These differences are largely attributed to geochemical characteristics of their source areas in this study.

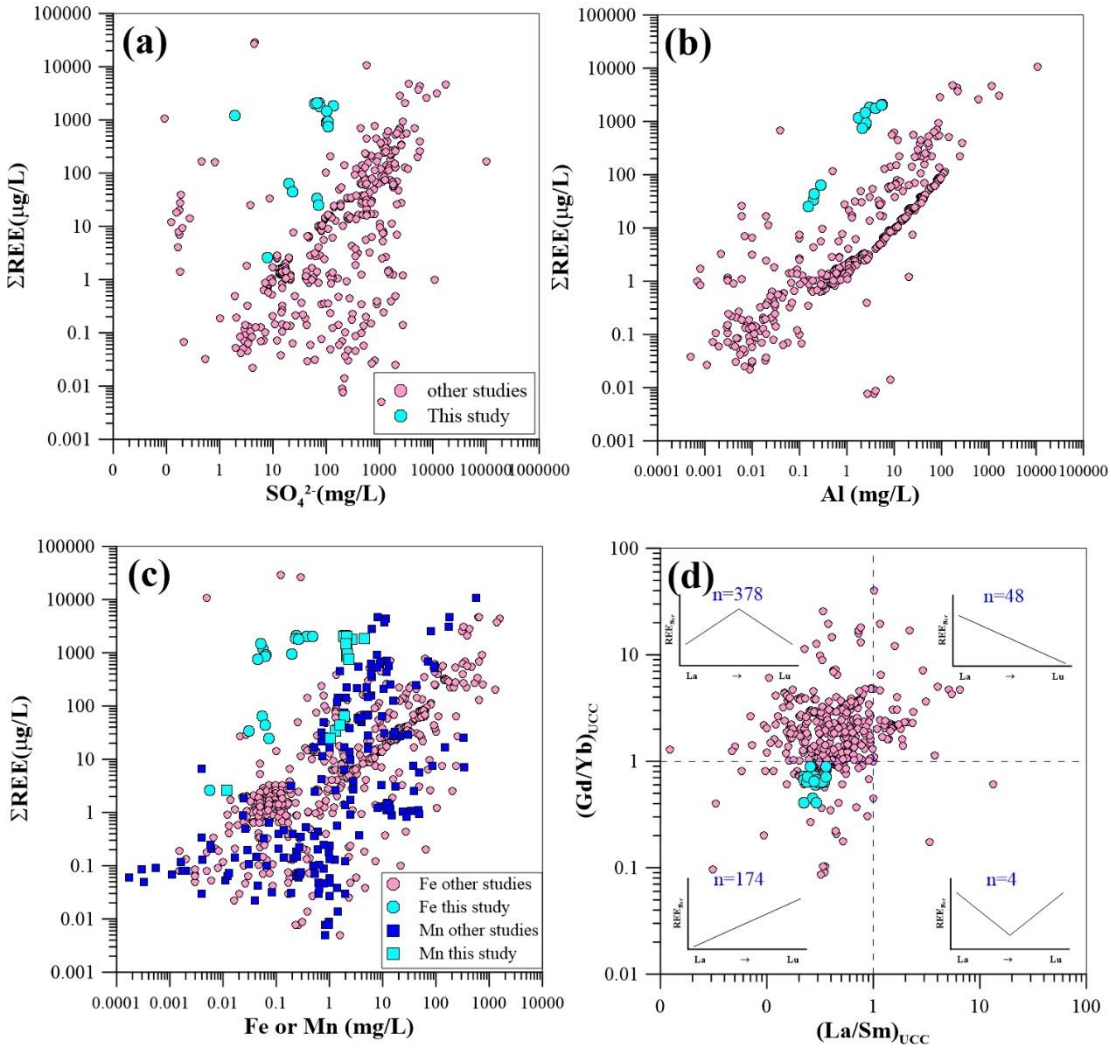

Figure 8 Relationship between total REE (∑REE) and SO_4^{2-} (a), Al (b), Fe and Mn (c) concentrations, and distinct fractionations of REE (d) (Other studies including Miekeley et al. (1992), Auqué et al. (1993, 1994), Johannesson and Lyon (1995), Elbaz-Poulichet and Dupuy (1999), Leybourne et al. (2000), Worrall and Pearson (2001), Protano and Riccobono (2002), Janssen and Verweij (2003), Merten and Büchel (2004), Bozau et al. (2004), Wood et al. (2005), Olías et al. (2005), Zhao et al. (2007), Silva et al. (2009), Pérez-López et al. (2010), Romero et al. (2010), Sun et al. (2012a, b), Borrego et al. (2012), Sharifi et al. (2013), Soltani et al. (2014), Yi et al. (2016), Li and Wu (2017), Stewart et al. (2017),Vass et al. (2019), Ogawa et al. (2019), Migaszewski et al. (2019) and Lozano et al. (2020a)) .

Table 5 REE concentrations (μg/L) in AMD reported in different countries

mine site	pH	REE (μg/L)	reference
Tharsis mine, Spain	-0.2-5.3, average=2.5	1-8896, average=1746	Moreno-Gonzaléz et al. (2020)
Erdenet mining area, Mongolia	7.4-8.9, average=8.1	3-11 ng/L, average=7	Munemoto et al. (2020)
Coal mine, China	2.7-4.6, average=3.1	118-926, average=418	Li and Wu (2017)
Wiśniówka mine, Poland	1.7-2.8, average=2.2	993-6288, average=3505	Migaszewski et al. (2016)
Iberian Pyrite Belt, Portugal	2.1-2.4, average=2.2	118-373, average=218	Pérez-López et al.(2010)
Santa Lucia mine, Cuba	2.5-2.8, average=2.6	35-530, average=256	Romero et al. (2010)
Lower Lusatia, Germany	2.5-6.7, average=3.3	2-932, average=248	Bozau et al. (2008)
REE Mine, China	4.6–7.4, average=6.1	0.17–13046, average=1596	Hao et al. (2016)
Berkley Pit Lake, United States	2.4	2688-2914, average=2774	Gammons et al. (2003)

4.2 REE+Y mobility

Abundances and distributions of REE+Y in acid waters are highly dependent on the REE+Y-bearing mineral phases in the bedrocks. Weathering and dissolution of bedrocks is a main pathway mobilizing REE+Y into solutions. Plots of UCC-normalized REE+Y patterns of rock samples show slight enrichment of HREE over LREE. Sediment samples show evident HREE-enriched normalized patterns (Fig. 5), and similar HREE enrichment characteristics are found in MW and NDT samples as well (Fig. 4a and c). Therefore, the acid waters have similar UCC-normalized patterns to those of sediments rather than rocks, which means that the HREE enrichments in MW probably result from the sediment signatures in this area, but unlikely from the rock signatures. The higher degrees of HREE enrichment in sediments relative to rocks suggest that REE+Y have fractionated during weathering of parent rocks. Therefore, after REE+Y as well as other metal elements (i.e. Fe, Mn and Al) are initially mobilized from the rocks, the majority of them are sorbed onto the

surfaces of sediments/soils which developed from rocks. During the process, the source-rock composition regulates HREE enrichment in sediments. When acid leaching occurs, the sorbed REE+Y are readily eluted from the surfaces of sediment. This secondary mobilization is unexpected to significantly fractionate REE+Y in acid waters for two possible reasons: (i) sulfate complex and free ion are the main solution species (Wood, 1990), as indicated by speciation calculations (Figs. 4 b and d); REE+Y association with sulfate is not believed to highly modify REE+Y patterns in aqueous solutions owing to the relatively unchangeable of REE+Y-sulfate formation constants (Schijf and Byrne, 2004; Wilkin et al., 2020); (ii) REE+Y re-adsorption onto mineral phases is quite limited. This is due to the general low pH values (< 4) in the MW samples, where REE+Y behave conservatively even though Fe oxyhydroxides are present (Verplanck et al., 2004). Pourret and Davranche (2013) showed that REE+Y were insignificantly bound to hydrous Mn oxide at pH of <4. These results indicate that the whole eluted REE+Y are ultimately discharged into streams/creeks, and are transported in forms of sulfate complex and free ions until solution conditions become neutral or weakly alkaline. Consequently, REE+Y originally triggered from the parent rocks and accumulated in sediments by adsorption directly contributes to REE+Y in acid waters, and sulfate complexation and free ion forms preserve HREE enrichment patterns.

4.3 Control on REE+Y signatures

4.3.1 REE+Y concentrations

Concentrations of REE+Y in the investigated acid waters are controlled by the bulk solution chemistry and co-precipitation of secondary minerals. A negative correlation exists between pH values and ΣREE+Y concentrations. The lowest pH occurring in MW favors dissolution of REE+Y-containing minerals in rocks and leaching of REE+Y from sediments (Dia et al., 2000; Worrall and Pearson, 2001; Janssen and Verweij, 2003). This controls REE+Y concentrations in acid waters from source areas, as reflected by high ΣREE+Y abundance in MW and NDT samples

where pH values below 4.9 prevail (Table 2). A decrease in ΣREE+Y concentrations in CPT samples is due to REE+Y scavenging via sorption and/or co-precipitation of secondary minerals resulting from increasing solution pH values to greater than 7.4. Trends of Fe, Al and SO_4^{2-} concentrations are consistent with those of ΣREE+Y concentrations with water flowing (Fig. 3a), indicating that Fe- and Al-bearing minerals are possible secondary phases immobilizing REE+Y from CPT samples. Results of XRD support that ferrihydrite and schwertmannite are the most plausible minerals which act as the sinks of aqueous REE+Y. These minerals have been determined in sludge samples (Fig. S3), and have been suggested to be the most common minerals precipitated from AMD during neutralization processes (Lozano et al., 2020). The dominant Fe species shifts from Fe(II) in MW and NDT samples to Fe(III) in CPT (Fig. 3a), suggesting that the formation of ferrihydrite and schwertmannite may occur following Eqs. (1) and (2).

$$4Fe^{2+} + O_2 + 10H_2O = 4Fe(OH)_3(s) + 8H^+ \quad (1)$$

$$8FeSO_4 + 2O_2 + (4 + m)H_2O = Fe_8O_8(OH)_mSO_n + (8-n)SO_4^{2-} + 2(8-n)H^+ \quad (2)$$

The impact of sorption and co-precipitation on ΣREE+Y concentrations is reflected by positive Y/Ho anomalies. Yttrium has the same charges and similar ionic radii to Ho. However, Y is thought to behave differently from Ho during sorption and co-precipitation with Ho having greater affinities than Y for surface complexes (Bau, 1999), and thus leads to fractionations between the two elements (Nozaki et al., 1997; Möller et al., 1998). The prevailing positive Y/Ho anomaly observed in water samples implies that sorption of REE+Y readily occurs during neutralization processes. Higher Y/Ho values are found in CPT samples (1.70 to 1.81) as compared to MW (1.14 to 1.53) and NDT (1.21 to 1.36) samples. This is attributed to intense sorption or/and co-precipitation of REE+Y in CPT samples, which is governed by solution pH values. Indeed, ΣREE+Y concentrations are negatively correlated with Y/Ho anomalies (R^2=0.66), showing that low-pH conditions are not the most favorable for REE+Y sorption. Results of field studies indicated that Y/Ho anomaly could be a tracer for understanding REE+Y sorption in groundwater (Tweed et al., 2006), although the

obtained samples were weakly alkaline. The great affinities for REE+Y to amorphous Fe oxyhydroxides could be achieved by means of adsorption and/or co-precipitation (De Carlo et al., 1998; Liu et al., 2017). Aluminum oxyhydroxides have been shown to effectively remove REE+Y from acid thermal water when it's neutralized to pH values of <6 (Ogawa et al., 2019). More recently, sorption behaviors of REE+Y onto schwertmannite were studied by Lozano et al. (2020a, b), showing that lanthanides sorption increased from pH 5to 6.5. It should be noted that changes of REE+Y concentrations may also be coupled to scavenging of Mn oxyhydroxides, which has a sorption edge as low as pH of 4 and a complete sorption at pH around 8 (Pourret and Davranche, 2013), although this mineral is not detected by XRD in sludge samples due to its low content in this study. Therefore, dissolved REE+Y concentrations are mainly determined by acidification-enhanced dissolution/leaching and scavenging of secondary minerals precipitated from aqueous solutions.

4.3.2 REE+Y patterns

All water samples exhibit enrichments in HREE relative to LREE when normalized to UCC (Fig.4). This fractionation patterns are inconsistent with the general enrichment in MREE over LREE and HREE observed in AMD worldwide (Pérez-López et al. 2010; Grawunder et al., 2015; Ayora et al., 2016; León et al., 2021). However, the REE+Y patterns of acid waters are still of diversity. HREE (Medas et al., 2013) and LREE (Bozau et al., 2004) enrichment have been found in other studies. Enrichments of both HREE and MREE in acidic systems have been shown as well (Gammons et al., 2003; Sharifi et al., 2013; Migaszewski et al., 2014). Indeed, among the 604 acid and acid water-impacted water samples documented in previous researches, 63% (n=378) and 29% (n=174) are characterized by MREE and HREE enrichment, as constrained by $(La/Sm)_{UCC}$ and $(Gd/Yb)_{UCC}$ fractionation measures. The remaining samples are enriched in LREE (n=48) or depleted in MREE (n=4) (Fig. 8d). Our results indicate that all samples are located in quadrant four, showing HREE enrichment. This fractionation pattern reported here are thought to

result from inheritance of sediment REE+Y signatures and solution complexations. The possible mechanisms are addressed as follow.

The flat UCC-normalized REE+Y pattern of parent rock indicates that it is not a direct cause for HREE enrichment in acid waters, whereas it can be sources of REE+Y contributing to acid waters via weathering and leaching. This has been discussed above. Generally, natural waters have distinct normalized REE+Y patterns when interacted with different rock types (Duvert et al., 2015). Cases have been reported that REE+Y patterns in circumneutral waters directly inherit from rocks that they interact with (Banner et al., 1989), and the patterns change with water flowing due to influences of (bio)geochemcial processes. However, the present study probably shows that REE+Y patterns are at a late stage of outflow discharges from the mine site. Therefore, it is impossible that there is a direct relationship between the REE+Y patterns in the acid waters and those in the parent rock.

The effect of organic matter on the formation of HREE enrichment waters can be ruled out due to the low DOC concentrations, which are generally below 3.2 mg/L with exceptions of sample CPT3 and CPT4. Preferential complexation of MREE relative to LREE and HREE with humic acid could lead to MREE-enriched patterns in alkaline waters (Wood, 1993; Pourret et al., 2007), which is the case reported by Munemoto et al. (2020), but not for the present study. The SEM results of filter residuals show no substantial REE+Y in forms of particulate (>0.22 μm) (Fig. 6). Hence, the REE+Y are mostly truly dissolved in acid waters and the particulates are unimportant to control the REE+Y fractionation patterns. Similar cases have been reported by Olías et al. (2018), indicating that REE+Y mainly occurred as dissolved fraction at pH below 4, and only when pH increases to greater than 7 can particulate REE+Y be observed in waters.

Scavenging of Fe and Al oxyhydroxides are supposed to occur for REE+Y. But the contribution of this process to HREE enrichment is only restricted to CPT samples, because only a weakly negative relationship (R^2=0.22) between ΣREE+Y concentrations and $(Yb/Nd)_{UCC}$ values is observed in CPT samples. The low pH values (<4; except for NDT1) in MW and NDT samples are not favorable for the

formation of Fe and Al oxyhydroxides as well, whereas ionic forms of Fe and Al are expected (Ogawa et al., 2019). Moreover, coefficients of distribution of the REE+Y between solids consisting of Al and Fe oxyhydroxides and water show a very weak increase across lanthanide series at pH of 6.3 to 6.8 (Lozano et al., 2020a). It reflects that REE+Y fractionation owing to adsorption or/and co-precipitation by Fe and Al oxyhydroxide in the study is insignificant.

Solution complexation is insufficiently enough to significantly fractionate REE+Y in the MW and NDT samples, but may impact REE+Y patterns in CPT and WW samples. Although SO_4^{2-} complexes and free ions are the dominate lanthanide species in MW and NDT sample, SO_4^{2-} is almost equally strong for all REE+Y, showing no preferential complexation of individual lanthanide (Wood, 1990). Constants of REE- NO_3^- complexation are higher for LREE than HREE (Millero, 1992), suggesting a preferential complexation of LREE over HREE. This does not make for HREE enrichment in waters either. Complexation to CO_3^{2-} could contribute to formation of HREE enrichment in CPT and WW due to preferential stabilization of HREE relative to LREE. This mechanism has been demonstrated to be responsible for HREE enrichment in natural alkaline waters (Liu et al., 2016). The preferential sorption of positively charged $REECO_3^+$ by negatively charged surfaces under neutral to weakly alkaline conditions may also lead to HREE enrichment (Guo et al., 2010). Other ligands including OH^-, PO_4^{3--}, F^- and Cl^- tend to preferentially complex HREE, but their low speciation predicted by the model or/and low concentrations exclude the possibility of HREE enrichment caused by solution complexation.

In consequence, the clear resemblance between REE+Y patterns in sediments and those in acid waters indicates that the aqueous REE+Y patterns are probably controlled by the characteristics of REE+Y source areas, and the patterns remain relatively unchangeable with water flowing irrespective of precipitation of secondary minerals due to a rise of pH values. A model can be developed as to the formation of HREE enrichment pattern in acid waters. (i) thick zones of clay rich sediment/soil would develop above the granites during weathering process (Van Gosen et al., 2014), as suggested by the common presence of kaolinite that determined by XRD (Fig. S3).

(ii) The mobilized REE+Y are initially adsorbed onto sediments, and a preferential accumulation of HREE by the metal oxides and/or clay minerals containing in sediments leads to HREE enrichment in sediments (Aström, 2001). This is reflected by the presence of ferrihydrite, kaolinite, schwertmannite in sediment samples (Fig. S3) and higher contents of HREE such as Gd, Er and Dy being detected by SEM in sediments (Fig. 7). (iii) The acid mining process leaches previously adsorbed REE+Y into aqueous solutions, giving rise to enrichments of HREE relative to LREEs in acidic waters (Leybourne et al., 2000; Migaszewski et al., 2016). No substantial variability of REE+Y patterns over plant treatments are for a large part due to REE+Y source controls. The origins of REE+Y patterns in acid water remain debatable. Studies suggest that they originate from REE+Y-rich soil waters leached from acid soils (Åström, 2001), while others attributed them to sulfides (Pérez-López et al., 2010) or dissolution of parent rock minerals (Cánovas et al., 2020). Ferreira da Silva et al. (2009) results show that REE of mining wastes in Lousal mine area result from the mixing of sulfides and host rocks, which is also part of arguments presented by Pérez-López et al. (2010). The dispersion of REE+Y patterns observed in AMD collected from 30 mining districts of the IPB was suggested to be controlled by local lithology and mineralogy (Léon et al., 2021). Similarly, the HREE enrichment patterns of acid waters shown in this study is a consequence of leaching of HREE-rich sediments developing from host rock.

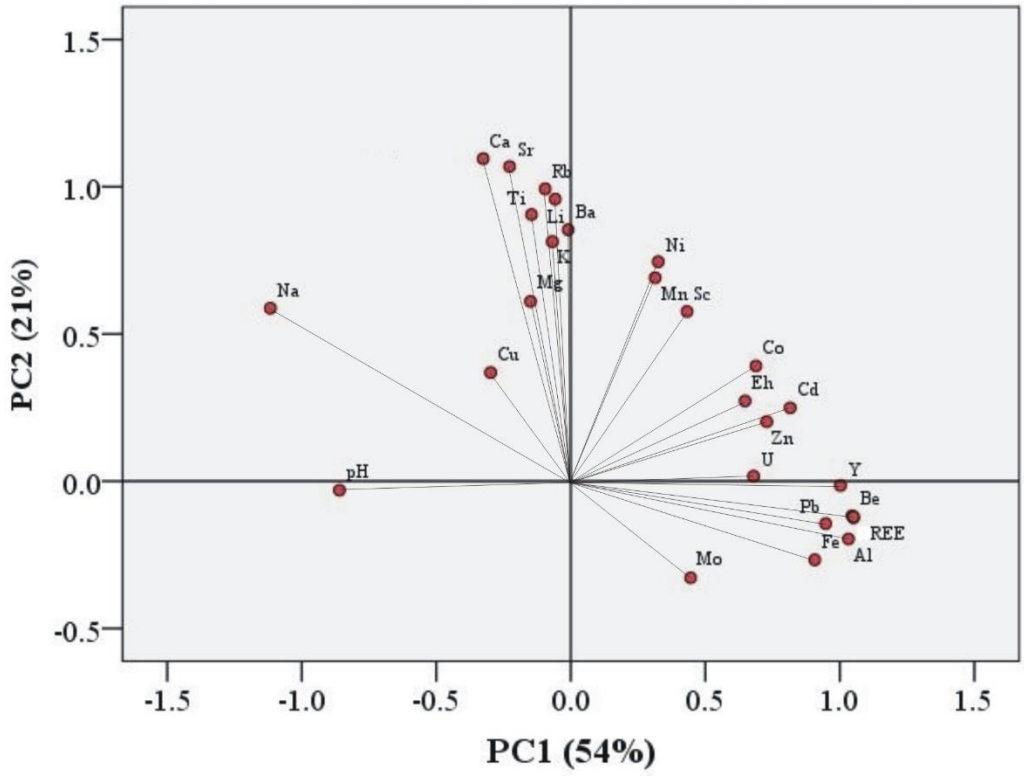

Figure 9 Principal component analysis (PCA) for all water samples

Principal component analysis (PCA) is applied to verify the fact. As shown in Fig. 9, two principal components with eigenvalue greater than 1 are obtained. The first component explains 54% of total variance of the data set and probably is related the mobility of various elements under the acidic conditions of the mine site. The preferentially mobilized elements are located in the positive field and the latterly mobilized elements in the negative field. The second component explains 21% of total variance and may represent acid leaching process in relation to the lithology that releases the different elements into acid waters. This hypothesis is generally consistent with the principal analysis results obtained by León et al. (2021), suggesting that the lithology of mine site played an important role in releases of REE+Y into the AMD. In this scenario, elements located in the positive field are mostly likely derived from acid dissolution of the host rock, such as Li, Sr, Mn, Ca, Mg, Ti, Ni, Co, Cd and U. The Eh also remains in this field, showing that the dissolution is influenced by redox environment. On the other hand, REE+ Y as well as Fe, Al, Pb, Be and Mo are located in the negative field, indicating that these elements mainly

come from leaching of sediments and are strongly associated with pH values, as the parameter is found to be in the same part of these elements. The only exception is Sc which remains in the positive field. Different behaviors of Sc with respect to the REE+Y at low pH may explain this phenomenon (Lozano et al., 2020). Thus, results of PCA further support that normalized REE+Y patterns are importantly controlled by geology of study area.

4.3.3 Ce anomalies

A narrow range of Ce anomalies (Ce/Ce*: 0.21 to 0.29) is observed in all water samples (Fig. 9). The negative Ce anomalies probably are originated from sediment REE+Y signatures, in which negative Ce anomalies are evident (0.61 to 0.79). Oxidation of soluble Ce(III) to insoluble Ce(IV) that is readily precipitate as CeO_2 and/or $Ce(OH)_4$ has been commonly recognized as a mechanism immobilizing Ce and resulting in negative Ce anomalies in aqueous solution. This process may have occurred when REE+Y either are initially mobilized from host rock or are secondarily mobilized from sediments. The lower Ce/Ce* values in sediments than rocks support the former to be a more plausible process generating negative Ce anomalies in acid waters. It is unlikely that redox process plays a dominate role in the development of negative Ce anomalies over acid water flow, since Ce anomalies keep relatively constant in all acid water samples despite the redox conditions are variable. Indeed, stability fields concerning relevant Ce species show that MW and NDT samples are located in Ce(III) domain, while CPT and WW sample in CeO_2 domain. This indicates that Ce would initially occur as free cation ion when it was leached from sediments, and it tends to be in forms of CeO_2 as pH increases and Eh decreases. In this respect, theoretically, oxidative scavenging of Ce by Fe oxyhydroxides and/or Mn oxides due to co-precipitation of these secondary minerals may occur in CPT samples (Ohta and Kawabe, 2001; Takahashi et al., 2007). However, the process could not be a dominate control on negative Ce anomalies as well, because the Ce/Ce* values in CPT samples are comparable to those of MW and NDT samples (Fig. 9a), despite

that Fe and Mn concentrations decrease substantially with acid waters flowing downwards (Fig. 3a). Furthermore, the SEM results show that no substantially higher contents of Ce than other REE+Y are observed in sludge samples (Fig. 7). Therefore, the negative Ce anomalies are suggested to be largely controlled by REE+Y sources in sediments. It's worthwhile to note that the role of source composition in development of Ce anomalies would be complexed by redox change, adsorption on particle surfaces, organic complexation, microbial-mediated activities, and preferential incorporation into secondary minerals (Dia et al., 2000; Protano and Riccobono, 2002; Pourret et al., 2007; Tanaka et al., 2010). Both negative and positive Ce anomalies in acid waters have been reported previously (Gammons et al., 2003; Olías et al., 2005) (Fig. 9b). Smedley et al. (1991) argued that Ce anomalies in slightly acidic groundwaters (5-6.8) were related to rock aquifer-source, and their water samples exhibited similar REE+Y patterns to those of rocks composed of granites and metasediments. Therefore, the occurrences of Ce anomalies found in acid waters are most likely source-sediment inherited characteristics rather than arising from the process-related oxidative precipitation of Ce in waters.

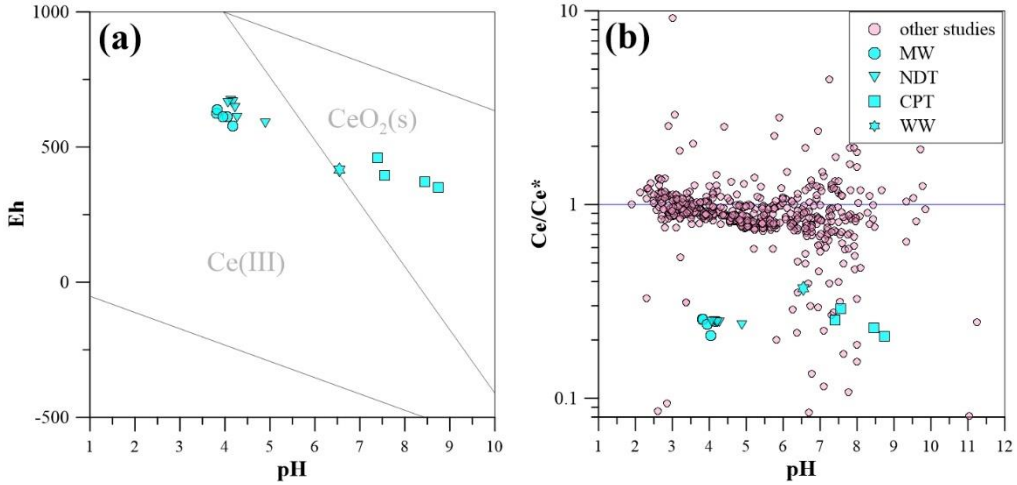

Figure 10 (a): Eh-pH diagram of Ce; (b) relationship between pH and Ce/Ce* (data shown in panel b are the same as used in Fig. 8)

4.4 Implication for REE+Y recovery

Although AMD has been flagged as an environmental concern globally due to its great hazard to ecosystems, it's a critically potential secondary source of REE+Y as well as coexisting metal elements which are of economic interest, if control and treatment are appropriately implemented. Neutralization of acidity constitutes a promising opportunity for recovering REE+Y from acid waters. As shown in this study, REE+Y are efficiently sequestrated from CPT samples, where pH values are increased to greater than 7.4. Correspondingly, high levels of REE+Y have been found in sludge samples, and their concentrations are higher than those of surface sediments. The yield of REE+Y that are potentially recoverable from acid waters has been calculated by the difference between loads of REE+Y in pristine acid waters and effluents of the treated waters. The loads of REE+Y are obtained by multiplying plant treatment capacity to the elemental concentrations in studied waters. Results show that the recoverable ∑LREE and ∑HREE range between 1116 and 3373 g/day, and between 1288 and 3764 g/day, contributing between 34% and 38%, and between 38% and 42% of the total ∑REE+Y, respectively (Fig. 11). The recoverable Y ranges between 793 and 2348 g/day (20% to 28%). The highest total recoverable value occurs at the location of MW5, which is nearest the inlet of WTP (Fig. 1).

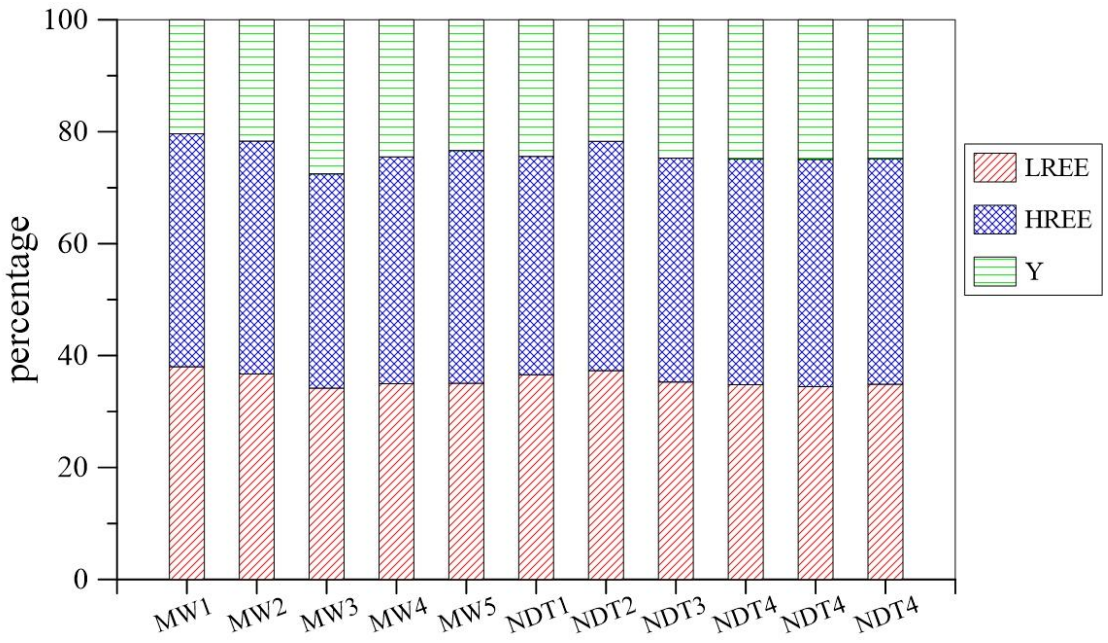

Figure 11 The proportion of potentially recoverable REE+Y in MW and NDT samples

It must be noted that the profitability of REE+Y recovery from AMD depends on their amounts born in AMD, the cost of separation and extraction, and the proportion of REE+Y in AMD (Léon et al., 2021). Hence, the high proportions of HREE found in this area makes recovery of REE+Y from the acid waters significantly attractive, considering HREE are more precious compared to LREE and are largely restricted to South China. The large differences in lanthanide price (SMM, 2020) derive studies focused on selective recovery of REE+Y from ADM and their treatment sludge. A preferential retention of REE+Y from AMD treatment process were reported in coal mines (Stewart et al. 2017; Hedin et al., 2019). The availability of recovering REE+Y as well as other critical metals like Cu, Zn and Ni from acid mine leachate and precipitates were documented by Zhang and Honaker (2018). Ayora et al. (2016) studied the recovery of REE+Y from passive remediation systems of AMD system with two substrate- (schwertmannite and basaluminite) based treatments, showing that AMD remediation process serves as a suitable REE+Y source. Biochar may server as a potential sorbent to immobilize these metals in aqueous solution where pH value is low to 3 (Pourret and Houben, 2018). In all, the practical examples of

REE+Y recovery from AMD render an environmental problem worthwhile as a source of raw materials, considering finding alternative sources of REE+Y is in pressing need and an increasing demand for these critical metals, particular for the countries without primary deposits.

5. Conclusions

This study investigates the geochemistry of rare earth element (REE) and yttrium (REE+Y) in acid mine drainage (AMD). Elevated concentrations of REE+Y are observed in the pristine mine water (MW, average 4115 μg/L) with a range of 3820 to 4301 μg/L and pH values of 3.8 to 4.2. A progressive decrease in REE+Y concentrations occur with MW flowing through nitrification-denitrification (NDT, average 2208 μg/L) and coagulating-precipitation treatment procedures (CPT, average 118 μg/L). However, as compared to REE+Y concentrations in well water (WW) collected downgradient of the mine site, MW, NDT and CPT samples have 1 to 3 orders of magnitude higher values. The negative correlation between REE+Y concentrations and pH values with a relationship coefficient (R^2) of 0.72 indicate that REE+Y are primarily derived from an enhanced acidic dissolution of minerals in the source area. XRD detection shows that muscovite, kaolinite and feldspar are possible REE+Y-bearing minerals. Upper Continental Crust (UCC)-normalized REE+Y patterns are characterized by heavy REE (HREE) enrichment over light REE (LREE) and negative Ce, as indicated by values of $(Yb/Nd)_{UCC}$ (average 8.05) and Ce/Ce* (average 0.25). The similarity of HREE-enriched patterns exhibited by AMD to those of sediment suggests a major role of sediments source in controlling REE+Y signatures of AMD. A preferential precipitation of LREE over HREE during the plant treatment process makes limited contribution to HREE enrichment in AMD, because the degree of HREE enrichment changes slightly and Ce anomalies keep relatively constant in MW, NDT and CPT samples. Results of XRD and SEM-EDS examination indicate that kaolinite, schwertmannite and ferrihydrite are the main hosts of REE+Y in sediments. Therefore, HREE-enrichment patterns in AMD result from preferential

leaching of HREE from sediment under the conditions of mine site. Free cation and sulfate complexes, which dominate REE+Y species in MW and NTD samples, facilitates the transport of REE+Y and preserves REE+Y patterns with AMD flow. Carbonate complexation accounts for HREE enrichment as well in CPT and WW samples. The loads of LREE and HREE in AMD are calculated to range between 1116 g/day and 3373 g/day, and between 1288 g/day and 3764 g/day, respectively, which shows great potential for REE+Y recovery from AMD.

Acknowledgments

This investigation has been funded by National Natural Science Foundation of China (No. 41902243), Natural Science Foundation of Jiangxi province, China (20202BABL211018). East China University of Technology Research Foundation for Advanced Talents (Nos. DHBK2019094 and SHT201901).

References

Akcil, A., Koldas, S. 2006. Acid Mine Drainage (AMD): causes, treatment and case studies. J. Clean. Prod. 14 (12- 13), 1139-1145.

Auqué, L. F., Tena, J. M., Mandodo, J. M., Gimeno, M. J., Zamora, A. 1994. Especiación de tierras raras en las soluciones ácidas y neutras del sistema de drenaje del arroyo del val (zaragoza). Estudios Geológicos. 50(3-4). (In French with English abstract)

Auqué, L. F., Tena, J. M., Gimeno, M. J., Mandado, J., Zamora, A.,Julián, P. L. 1993. Distribución de tierras raras en soluciones y coloides de un sistema natural de aguas ácidas (Arroyo del Val, Zaragoza). Estudios Geológicos, 49(1-2), 41-48. (In French with English abstract)

Åström, M., Corin, N. 2003. Distribution of rare earth elements in anionic, cationic and particulate fractions in boreal humus-rich streams affected by acid sulphate soils. Wat. Res. 37, 273-280.

Åström, M. 2001. Abundance and fractionation patterns of rare earth elements in

streams affected by acid sulphate soils. Chem. Geol. 175, 249-258.

Ayora, C., Macias, F., Torres, E., Lozano, A., Carrero, S., Nieto, J. M., Perez-Lopez, R., Fernandez-Martinez, A., Castillo-Michel, H., 2016. Recovery of rare earth elements and yttrium from passive-remediation systems of acid mine drainage. Environ. Sci. Technol. 50, 8255-8262.

Banner, J. L., Wasserburg, G. J., Dobson, P. F., Carpenter, A. B., Moore, C. H. 1989. Isotopic and trace element constraints on the origin and evolution of saline groundwaters from central Missouri. Geochim. Cosmochim. Acta 53, 383-398.

Bau, M. 1999. Scavenging of dissolved yttrium and rare earths by precipitating iron oxyhydroxide: Experimental evidence for Ce oxidation, Y-Ho fractionation, and lanthanide tetrad effect. Geochim. Cosmochim. Acta 63, 67-77.

Binnemans, K., Jones, P. T., Blanpain, B., Van Gerven, T., Yang, Y., Walton, A., Buchert, M. 2013. Recycling of rare earths: a critical review. J. Clean. Prod. 51, 1-22.

Borrego, J., Carro, B., Lopez-Gonzalez, N., Rosa, J., Grande, J. A., Gomez, T. 2012. Effect of acid mine drainage on dissolved rare earth elements geochemistry along a fluvial estuarine system: the Tinto-Odiel Estuary (S.W. Spain). Hydrol. Res. 43(3), 262-274.

Bozau, E., Leblanc, M., Seidel, J. L., Strk, H. J. 2004. Light rare earth elements enrichment in an acidic mine lake (lusatia, germany). Appl. Geochem. 19(3), 261-271.

Cánovas, C. R., Chapron, S., Arrachart, G., Pellet-Rostaing, S., 2019. Leaching of rare earth elements (REEs) and impurities from phosphogypsum: a preliminary insight for further recovery of critical raw materials. J. Clean. Prod. 219, 225-235.

De Carlo, E. H.; Wen, X. Y.; Irving, M. 1998. The influence of redox reactions on the uptake of dissolved Ce by suspended Fe and Mn oxide particles. Aquat. Geochem. 3, 357-389.

Delgado, J., Perez-Lopez, R., Galvan, L., Nieto, J. M., Boski, T. 2012. Enrichment of rare earth elements as environmental tracers of contamination by acid mine drainage in salt marshes; A new perspective. Mar. Pollut. Bull. 64, 1799-1808.

Dia, A., Gruau G., Olivié-Lauquet G., Riou C., Molénat J. and Curmi P. 2000. The distribution of rare earth elements in groundwaters: Assessing the role of source-rock composition, redox changes and colloidal particles. Geochim. Cosmochim. Acta 64, 4131-4151.

Duvert, C., Cendón, D.I., Raiber, M., Seidel., J., Cox, M. E. 2015. Seasonal and spatial variations in rare earth elements to identify inter-aquifer linkages and recharge processes in an Australian catchment. Chem. Geol. 369, 83-97.

Elbaz-Poulichet, F., Dupuy, C. 1999. Behaviour of rare earth elements at the freshwater–seawater interface of two acid mine rivers: the tinto and odiel (andalucia, spain). Appl. Geochem. 14(8), 1063-1072.

Elderfield, J., Upstill-Goddard, R., Sholkovitz, E. R. 1990. The rare earth elements in rivers, estuaries and coastal seas and their significance to the composition of ocean waters. Geochim. Cosmochim. Acta 54, 971-991.

Ferreira da Silva, E., Bobos, I., Matos, J. X., Patinha, C., Reis, A. P., Cardoso Fonseca, E. 2009. Mineralogy and geochemistry of trace metals and REE in volcanic massive sulfide host rocks, stream sediments, stream waters and acid mine drainage from the Lousal mine area (Iberian Pyrite Belt, Portugal). Appl. Geochem. 24, 383-401.

Gammons, C. H., Wood, S. A., Jonas, J. P., Madison, J. P. 2003. Geochemistry of rare earth elements and uranium in the acidic Berkeley Pit Lake, Butte, Montana. Chem. Geol. 198, 269-288.

Gimeno, M. J., Auqué, L. F., Nordstrom, D. K. 2000. REE speciation in low-temperature acidic waters and the competitive effects of aluminium. Chem. Geol. 165, 167-180.

Grawunder, A., Lonschinski, M., Merten, D., Büchel, G. 2015. Rare earth elements as a tool for studying the formation of cemented layers in an area affected by acid mine drainage. Appl. Geochem. 54:100-110.

Guo, H. M., Zhang, B., Wang, G. C., Shen, Z. L. 2010. Geochemical controls on arsenic and rare earth elements approximately along a groundwater flow path in the shallow aquifer of the Hetao Basin, Inner Mongolia. Chem. Geol. 270,

117-125.

Hao, X. Z., Wang, D. J., Wang, P. R., Wang, Y. X., Zhou D. M. 2016. Evaluation of water quality in surface water and shallow groundwater: a case study of a rare earth mining area in southern Jiangxi Province, China. Environ. Monit. Assess. 188(1), 24.

Hedin, B. C., Capo, R. C., Stewart, B. W., Hedin, R. S., Lopano, C. L., Stuckman, M. Y. 2019. The evaluation of critical rare earth element (REE) enriched treatment solids from coal mine drainage passive treatment systems. Int. J. Coal Geol. 208, 54-64.

Hummel, W., Berner, U., Curti, E., Pearson, F. J., Thoenen, T. Nagra/PSI Chemical Thermodynamic Data Base 01/01. Radiochim. Acta 2002, 90, 805-813.

Janssen, R. P. T., Verweij, W., 2003. Geochemistry of some rare earth elements in groundwater, Vierlingsbeek, The Netherlands. Water Res. 37, 1320-1350.

Johannesson, K. H., Lyons, W. B. 1995. Rare-earth element geochemistry of Colour Lake, an acidic freshwater lake on Axel Heiberg Island, northwest territories, Canada. Chem. Geol. 119(1-4), 209-223.

Johnson, D. B., Hallberg, K. B. 2005. Acid mine drainage remediation options: a review. Sci. Total Environ. 338 (1), 3-14.

Li, X. X., Wu, P. 2017. Geochemical characteristics of dissolved rare earth elements in acid mine drainage from abandoned high-as coal mining area, southwestern china. Environ. Sci. Pollut. R 24(1-3), 20540-20555.

Leybourne, L., Goodfellow, W. D., Boyle, D. R., Hall, G. M. 2000. Rapid development of negative Ce anomalies in surface waters and contrasting ree patterns in groundwaters associated with Zn-Pb massive sulphide deposits. Appl. Geochem. 15(6), 695-723.

Lozano, A., Ayora, C., Macías, F., Léon, R., Gimeno, M. J., Auqué, L. 2020a. Geochemical behavior of rare earth elements in acid drainages: modeling achievements and limitations. J. Geochem. Explor. 216, 106577.

Lozano, A., Ayora, C., Fernández-Martínez, A. 2020b. Sorption of rare earth elements on schwertmannite and their mobility in acid mine drainage treatments. Appl.

Geochem 113:104499.

Léon, R., Macías, F., Cánovas, C. R., Pérez-López, R., Ayora, C., Nieto, J. M., Olías, M. 2021. Mine waters as a secondary source of rare earth elements worldwide: the case of the Iberian Pyrite Belt. J. Geochem. Explor. 224, 106742.

Liu, W. S., Wu, L. L., Zheng, M. Y., Chao, Y. Q., Zhao, C. M., Zhong, X., Ding, K. B., Huot, H., Zhang, M. Y., Tang, Y. T., Li, C., Qiu, R. L. 2019. Controls on rare-earth element transport in a river impacted by ion-adsorption rare-earth mining. Sci. Total Environ, 660, 697-704.

Liu, H. Y., Guo, H. M., Wu, L. H. 2017. Rare earth elements as indicators of groundwater mixing in the North China Plain: A case study in the area of Hengshui city, China. Pro. Earth Plant. Sci. 17, 396-399.

Liu, H. Y., Pourret, O., Guo, H. M., Bonhoure, J. 2017. Rare earth elements sorption to iron oxyhydroxide: Model development and application to groundwater. Appl. Geochem. 87, 158-166.

Liu, H. Y., Guo, H. M., Xing, L. N., Zhan, Y. H., Li, F. L., Shao, J. L., Niu, H., Liang, X., Li, C. C. 2016. Geochemical behaviors of rare earth elements in groundwater along a flow path in the North China Plain. J. Asian Earth Sci. 117, 33-51.

Luo, Y. R., Byrne, R. H. 2004. Carbonate complexation of yttrium and the rare earth elements in natural waters. Geochim. Cosmochim. Acta 68, 691-699.

Marquez, J., Pourret, O., Faucon, M. P., Weber, S., Hoàng, T., Martinez, R. 2018. Effect of cadmium, copper and lead on the growth of rice in the coal mining region of Quang Ninh, Cam-Pha (Vietnam). Sustainability, 10, 1758

Medas, D., Cidu, R., Giudici, G. D., Podda, F. 2013. Geochemistry of rare earth elements in water and solid materials at abandoned mines in SW Sardinia (Italy). J. Geochem. Explor. 133, 149-159.

Merten, D., Büchel, G. 2004. Determination of rare earth elements in acid mine drainage by inductively coupled plasma mass spectrometry. Microchim. Acta 148(3-4), 163-170.

Miekeley, N., Jesus, H., Silveira, C., Linsalata, P., Morse, R. 1992. Rare-earth elements in groundwaters from the osamu utsumi mine and morro do ferro

analogue study sites, poços de caldas, Brazil. J. Geochem. Explor. 45(1-3), 365-387.

Migaszewski, Z. M., Gałuszka, A., Dołęgowska, S. 2019. Extreme enrichment of arsenic and rare earth elements in acid mine drainage: Case study of Wiśniówka mining area (south-central Poland). Environ. Pollut. 244, 898-906.

Migaszewski, Z. M., Gałuszka, A., Gowska, S. 2016. Rare earth and trace element signatures for assessing an impact of rock mining and processing on the environment: Wiśniówka case study, south-central Poland. Environ. Sci. Pollut. Res. 23, 24943-24959.

Migaszewski, Z., Gałuszka, A., Migaszewski, A. 2014. The study of rare earth elements in farmer's well waters of the Podwiśniówka acid mine drainage area (south-central Poland). Environ. Monit. Assessm. 186, 1609-1622.

Millero, F. J. 1992. Stability constants for the formation of rare earth inorganic complexes as a function of ionic strength. Geochim. Cosmochim. Acta 56, 3123-3132.

Munemoto, T., Solongo, T., Okuyama, A., Fukushi, K., Fukushi, K., Yunden, A., Batbold, T., Altansukh, O., Takahashi, Y., Iwai, H., Nagao, S. 2020. Rare earth element distributions in rivers and sediments from the erdenet Cu-Mo mining area, mongolia. Appl. Geochem, 123, 104800.

Möller, P., Dulski, P., Gerstenberger, H., Morteani, G., Fuganti, A. 1998. Rare earth elements, yttrium and H, O, C, Sr, Nd and Pb isotope studies in mineral waters and corresponding rocks from NW-Bohemia, Czech Republic. Appl. Geochem. 13 (8), 975-994.

Nordstrom, D. K., Blowes, D. W., Ptacek, C. J. 2015. Hydrogeochemistry and microbiology of mine drainage: an update. Appl. Geochem. 57, 3-16.

Nordstrom, D. K. 2011. Hydrogeochemical processes governing the origin, transport and fate of major and trace elements from mine wastes and mineralized rock to surface waters. Appl Geochem 26:1777-1791.

Nordstrom, D. K., Alpers, C. N. The geochemistry of acid mine waters. In The Environmental Geochemistry of Mineral Deposits: Chapter 6: Processes,

Methods and Health Issues; Plumlee, G.S., Logsdon, M.J., Eds.; Society of Economic Geologists: Littleton, CO, USA, 1999; pp. 133-160.

Nozaki, Y., Zhang, J., Amakawa, H. 1997. The fractionation between Y and Ho in the marine environment. Earth Planet. Sci. Lett. 148, 329-340.

Ogawa, Y., Ishiyama, D., Shikazono, N., Iwane, K., Hoshino, T., Kajiwara, M., Tsuchiya, N., Saini-Eidukat, B. Wood, S. A. 2019. Fractionation of rare earth elements (REEs) and actinides (U and Th) originating from acid thermal water during artificial and natural neutralization processes of surface waters. Geochim. Cosmochim. Acta 249: 247-262.

Ohta, A., Kawabe, I. 2001. REE(III) adsorption onto Mn dioxide and Fe oxyhydroxide: Ce(III) oxidation by Mn dioxide. Geochim. Cosmochim. Acta 65, 695-703.

Olías, M., Cánovas, C. R., Basallote, D. B., Lozano, A. 2018. Geochemical behaviour of rare earth elements (REE) along a river reach receiving inputs of acid mine drainage. Chem. Geol. 493, 468-477.

Olías, M., Cerón, J. C., Fernández, I., Rosa, J. D. L. 2005. Distribution of rare earth elements in an alluvial aquifer affected by acid mine drainage: the Guadiamar aquifer (SW Spain). Environ. Pollut. 135(1), 53-64.

Pourret, O., Houben, D. Characterization of metal binding sites onto biochar using rare earth elements as a fingerprint. Heliyon, 2018, 4, e00543.

Pourret, O., Davranche, M. 2013. Rare earth element sorption onto hydrous manganese oxide: A modeling study. J. Colloid interface Sci. 395, 18-23.

Pourret O., Davranche D., Gruau G., Dia A. 2007. Rare earth elements complexation with humic acid. Chem. Geol. 243, 128-141.

Protano, G., Riccobono, F. 2002. High contents of rare earth elements (REEs) in stream waters of a cu-pb-zn mining area. Environ. Pollut. 117(3), 499-514.

Pérez-López, R., Delgado, J., Nieto J. M., Márquez-García, B. 2010. Rare earth element geochemistry of sulphide weathering in the São Domingos mine area (Iberian Pyrite Belt): a proxy for fluid-rock interaction and ancient mining pollution. Chem. Geol. 276: 29-4.

Rodushkin, I., Paulukat, C., Pontér, S., Engström, E., Baxter, D. C., Sörlin, D.,

Pallavicini, N., Rodushkina, K. 2018. Application of double-focusing sector field icp-ms for determination of ultratrace constituents in samples characterized by complex composition of the matrix. Sci. Total Environ. 622-623, 203-213.

Romero, F. M., Prol-Ledesma, R. M., Canet, C., Alvares, L. N., Pérez-Vázquez, R. 2010. Acid drainage at the inactive santa lucia mine, Western Cuba: natural attenuation of arsenic, barium and lead, and geochemical behavior of rare earth elements. Appl. Geochem. 25(5), 716-727.

Sahoo, P. K., Tripathy, S., Equeenuddin, S. M., Panigrahi, M. K. 2012. Geochemical characteristics of coal mine discharge vis-à-vis behaviour of rare earth elements at Jaintia Hills coalfield, northeastern India. J. Geochem. Explor. 112, 235-243.

Schijf, J. Byrne R. H. 2004. Determination of $SO_4\beta_1$ for yttrium and the rare earth elements at I = 0.66 m and t = 25 °C-Implications for YREE solution speciation in sulfate-rich waters. Geochim. Cosmochim. Acta 68, 2825-2837.

Sharifi, R., Moore, F., Keshavarzi, B. 2013. Geochemical behavior and speciation modeling of rare earth elements in acid drainages at sarcheshmeh porphyry copper deposit, Kerman province, Iran. Chemie der Erde-Geochemistry, 73(4), 509-517.

Silva, E., Bobos, I., Matos, J. X., Patinha, C., Reis, A. P., Fonseca, E. C. 2009. Mineralogy and geochemistry of trace metals and REE in volcanic massive sulfide host rocks, stream sediments, stream waters and acid mine drainage from the Lousal mine area (Iberian Pyrite Belt, Portugal). Appl. Geochem. 24(3), 383-401.

Smedley, P. L. 1991. The geochemistry of rare earth elements in groundwater from the Carnmenellis area, southwest England. Geochim. Cosmochim. Acta 55, 2767-2779.

SMM. 2020. Shangai Metals Market. https://www.metal.com/ (accessed April 2021).

Soltani, N., Moore, F., Keshavarzi, B., Sharifi, R. 2014. Geochemistry of trace metals and rare earth elements in stream water, stream sediments and acid mine drainage from Darrehzar copper mine, Kerman, Iran. Water Quality, Exposure and Health, 6(3), 97-114.

Stewart, B. W., Capo, R. C., Hedin, B. C., Hedin, R. S. 2017. Rare earth element resources in coal mine drainage and treatment precipitates in the Appalachian Basin, USA. Int. J. Coal Geol. 169, 28-39.

Sun, H. F., Zhao, F. H., Zhang, M., Z., Li, J. Q. 2012a. Behavior of rare earth elements in acid coal mine drainage in Shanxi province, china. Environ. Earth Sci. 67(1), 205-213.

Sun, H. F., Zhao, F. H., Zheng, M., Li, H. Q. 2012b. Fractiontion patterns and influence mechanism of rare earth elements in acid mine drainage. J. China University Mining Technol. 41(2), 283-288. (In Chinese with English abstract)

Takahashi, Y., Manceau, A., Geoffroy, N., Marcus, M. A., Usui, A. 2007. Chemical and structural control of the partitioning of Co, Ce, and Pb in marine ferromanganese oxides. Geochim. Cosmochim. Acta 71(4), 984-1008.

Tanaka, K., Tani, Y., Takahashi, Y., Tanimizu, M., Suzuki, Y., Kozai, N., Ohnuki, T. 2010. A specific Ce oxidation process during sorption of rare earth elements on biogenic Mn oxide produced by Acremonium sp. Strain KR21-2. Geochim. Cosmochim. Acta, 74, 5463-5477.

Taylor, S. R. McClennan, S. M. 1988. The significance of the rare earths in geochemistry and cosmochemistry. In Handbook on the Physcis and Chemistry of the Rare Earths (eds. K. A. Gschneidner Jr and L. Eyring), Vol. 11, pp. 465-479, Elsevier, Amsterdam.

Tweed, S. O., Weaver, T. R., Cartwright, I., Schaefer, B. 2006. Behavior of rare earth elements in groundwater during flow and mixing in fractured rock aquifers: An example from the Dandenong Ranges, southeast Australia. Chem. Geol. 234, 291-307.

Van Gosen, B. S., Verplanck, P. L., Long, K. R., Gambogi, J., Robert, R., Seal, I. I. The Rare-Earth Elements: Vital to Modern Technologies and Lifestyles (No. 2014-3078). Available online: https://pubs.usgs.gov/fs/2014/3078/pdf/fs2014-3078.pdf (accessed on 5 April 2021).

Vass, C. R., Noble, A., Ziemkiewicz, P. F. 2019. The occurrence and concentration of

rare earth elements in acid mine drainage and treatment by-products: part 1—initial survey of the northern Appalachian coal basin. Mining, Metall. Explor. 36(5), 903-916.

Verplanck, P. L., Nordstrom, D. K., Taylor, H. E., Kimball, B. A. 2004. Rare earth element partitioning between hydrous ferric oxides and acid mine water during iron oxidation. Appl. Geochem. 19:1339-1354.

Wall, F. 2014. Rare earth elements. In: Gunn G. (Ed.) Critical Metals Handbook. John Wiley & Sons, Ltd., 312-339.

Wallrich, I. L., Stewart, B. W., Capo, R. C., Hedin, B. C., Phan, T. T. 2020. Neodymium isotopes track sources of rare earth elements in acidic mine waters. Geochim. Cosmochim. Acta 269, 465-483.

Wilkin, R. T., Lee, T. R., Ludwig, R. D., Wadler, C., Brandon, W., Mueller, B., Davis, E., Luce, D., Edwards, T. 2020. Rare-earth elements as natural tracers for in situ remediation of groundwater. Environ. Sci. Technol. 55(2). DOI: 10.1021/acs.est.0c06113.

Wood, S. A., Shannon, W. M., Baker, L. 2005. The Aqueous Geochemistry of the Rare Earth Elements and Yttrium. Part 13: REE Geochemistry of Mine Drainage from the Pine Creek Area, Coeur d'Alene river valley, Idaho, USA. Springer Netherlands.

Wood, S. A. 1993. The aqueous geochemistry of the rare-earth elements: critical stability constants for complexes with simple carboxylic acids at 25°C and 1 bar and their application to nuclear waste management. Eng. Geol. 34, 229-259

Wood, S. A. 1990. The aqueous geochemistry of the rare-earth elements and yttrium: 2. Theoretical predictions of speciation in hydrothermal solutions to 350°C at saturation water vapor pressure. Chem. Geol. 88:99-125

Worrall, F., Pearson, D. G. 2001. Water-rock interaction in an acidic mine discharge as indicated by rare earth element patterns. Geochim. Cosmochim. Acta 65(18), 3027-3040.

Yang, X. J., Li, A. J., Li, X. L., Wu, Y. D., Zhou, W. B., Chen, Z. H. 2013. China's ion-adsorption rare earth resources, mining consequences and preservation.

Environ. Dev. 8 (1), 131-136.

Yi, C. W., Chen, B. H., Li, W., Zhou, Y. M., Wang, Z. M., Zhang, J. T., Cheng, Y. Y., Zou, Z. H. 2016. Geochemical characteristics of rare earth elements in Dabaoshan acid mine drainages, Guangdong Province, China. Earth Environ. 44(1), 73-81. (In Chinese with English abstract)

Zhang, W., Honaker, R., 2020. Process development for the recovery of rare earth elements and critical metals from an acid mine leachate. Miner. Eng. 153, 106382

Zhang, J., Liu, C. Q. 2004. Major and rare earth elements in rainwaters from Japan and East China Sea: natural and anthropogenic sources. Chem. Geol. 209(3-4), 315-326.

Zhu, Z. Z., Liu, C. Q, Wang, Z. L., Liu, X. L., Li, J. 2016. Rare earth elements concentrations and speciation in rainwater from Guiyang, an acid rain impacted zone of southwest china. Chem. Geol. 442, 23-34.

Zhao, F., Cong, Z., Sun, H., Ren, D. 2007. The geochemistry of rare earth elements (REE) in acid mine drainage from the Sitai coal mine, Shanxi Province, North China. Int. J. Coal Geol. 70, 184-192.